HHS Public Access

Author manuscript

Cell Rep. Author manuscript; available in PMC 2019 October 28.

Published in final edited form as:

Cell Rep. 2019 October 08; 29(2): 332–346.e5. doi:10.1016/j.celrep.2019.09.011.

Dual and Opposing Functions of the Central Amygdala in the Modulation of Pain

Torri D. Wilson[1,2], **Spring Valdivia**[1,2], **Aleisha Khan**[1,2], **Hye-Sook Ahn**[1], **Anisha P. Adke**[1], **Santiago Martinez Gonzalez**[1], **Yae K. Sugimura**[1], **Yarimar Carrasquillo**[1,3,*]

[1]National Center of Complementary and Integrative Health, National Institutes of Health, Bethesda, MD, United States

[2]These authors contributed equally

[3]Lead Contact

SUMMARY

Pain perception is essential for survival and can be amplified or suppressed by expectations, experiences, and context. The neural mechanisms underlying bidirectional modulation of pain remain largely unknown. Here, we demonstrate that the central nucleus of the amygdala (CeA) functions as a pain rheostat, decreasing or increasing pain-related behaviors in mice. This dual and opposing function of the CeA is encoded by opposing changes in the excitability of two distinct subpopulations of GABAergic neurons that receive excitatory inputs from the parabrachial nucleus (PB). Thus, cells expressing protein kinase C-delta (CeA-PKCδ) are sensitized by nerve injury and increase pain-related responses. In contrast, cells expressing somatostatin (CeA-Som) are inhibited by nerve injury and their activity drives antinociception. Together, these results demonstrate that the CeA can amplify or suppress pain in a cell-type-specific manner, uncovering a previously unknown mechanism underlying bidirectional control of pain in the brain.

In Brief

The brain can bidirectionally influence behavioral responses to painful stimuli. Wilson et al identify a cellular mechanism underlying a pain rheostat system within the forebrain, with activation of CeA-Som neurons attenuating pain-related responses and increases in the activity of CeA-PKCδ neurons promoting amplification of pain-related behaviors following injury.

*Correspondence: yarimar.carrasquillo@nih.gov.

AUTHOR CONTRIBUTIONS

Conceptualization, Y.C.; Methodology, Y.C., T.D.W., and S.V.; Investigation, T.D.W., S.V., A.K., H.-S.A., A.P.A., S.M.G., Y.K.S., and Y.C.; Writing – Original Draft, Y.C.; Writing – Review & Editing, T.D.W., S.V., A.K., H.-S.A., A.P.A., S.M.G., and Y.K.S.; Supervision, Y.C.; Funding Acquisition, Y.C.

SUPPLEMENTAL INFORMATION

Supplemental Information can be found online at https://doi.org/10.1016/j.celrep.2019.09.011.

DECLARATION OF INTERESTS

The authors declare no competing interests.

INTRODUCTION

Over 100 million adults in the United States alone suffer from chronic pain and 25 million of these patients experience pain every day (Nahin, 2015). These statistics highlight the fact that chronic pain is still poorly treated and represents a major healthcare problem. Understanding the neurobiological mechanisms by which pain responses can be enhanced or suppressed is essential for the development of improved therapeutic options for chronic pain. The central nucleus of the amygdala (CeA) has received increasing attention in recent years as a nociceptive center in the brain that is ideally positioned to link experience, context, and emotional states with behavioral responses to painful stimuli in both normal and pathological states (Davis, 1994; Davis and Whalen, 2001; Neugebauer et al., 2004; Veinante et al., 2013; Zald, 2003). The CeA receives direct nociceptive inputs via the spino-ponto-amygdaloid pain pathway, as well as highly processed affective and cognitive polymodal information via the basolateral nucleus of the amygdala (Bernard and Besson, 1990; Bernard et al., 1989; Jasmin et al., 1997).

Consistent with the critical function of the CeA in pain modulation, recent studies have shown that pain-related plasticity in this brain region promotes hypersensitivity in pathological states (Bourbia et al., 2010; Carrasquillo and Gereau, 2007, 2008; Kolber et al., 2010; Min et al., 2011; Nation et al., 2018; Xie et al., 2017). Nociceptive inputs from the parabrachial nucleus (PB) to the CeA have also been recently shown to be essential for the conversion of nociceptive stimuli to defensive responses and for the subsequent formation of a threat memory (Han et al., 2015). Maladaptive changes in the CeA can, therefore, induce persistent hypersensitivity as well as alterations in affective behaviors, which are commonly comorbid in chronic pain conditions in both humans and rodents (Bushnell et al., 2013; Nahin, 2015; Veinante et al., 2013; Yalcin et al., 2011). In a contradictory manner, however, earlier studies demonstrated that the CeA is an important locus for analgesia, promoting pain reduction secondary to stress or pharmacological manipulations (Fox and Sorenson, 1994; Manning, 1998; Manning et al., 2001, 2003; Manning and Mayer, 1995a, 1995b). The mechanisms underlying these apparently dual and seemingly opposing functions of the CeA in pain modulation remain unknown.

Previous studies have shown that CeA neurons are physiologically, genetically, and functionally heterogenous (Janak and Tye, 2015). Despite the known cellular and functional heterogeneity in the CeA, studies of pain processing in this brain region have been limited to unidentified populations of cells and/or global manipulations that target all cells within the CeA. In this study, we dissected the function of subpopulations of cells within the CeA by taking advantage of molecular genetic approaches that allow us to fluorescently label and manipulate the activity of distinct CeA cell types based on their gene expression. We focused our studies on cells expressing either protein kinase C delta (CeA-PKCδ) or somatostatin (CeA-Som) because these constitute the majority of CeA neurons and represent largely nonoverlapping populations (Kim et al., 2017; Li et al., 2013). Using these cell-type-specific approaches, our experiments demonstrated that the CeA can function as a pain rheostat, amplifying or suppressing pain-related behaviors, and that the ability of the CeA to bidirectionally modulate pain is encoded by opposing changes in the excitability of CeA-PKCδ and CeA-Som cells.

RESULTS

Nerve-Injury-Induced ERK Activation and c-Fos Expression Are Preferentially Localized to CeA-PKCδ Cells

To test whether modulation of pain-related behaviors in the CeA is cell-type specific, we used the sciatic nerve cuff model of neuropathic pain (Benbouzid et al., 2008). The acetone test, Hargreaves test, von Frey filaments assay, and Randall Selitto test were used to measure sensitivity to cold, heat, tactile, and pinch stimulation of the hindpaw, respectively (Figure 1A). Paw responses to the different stimuli were measured 1–2 weeks after the sciatic nerve surgery. Consistent with previous reports (Benbouzid et al., 2008), cuff implantation produced robust hypersensitivity to all four modalities in the paw ipsilateral (Figure 1B), but not contralateral to the injury (Figure S1A).

CeA neurons are entirely GABAergic and receive nociceptive inputs from the PB via the spino-ponto-amygdaloid pathway (Bernard and Besson, 1990; Bernard et al., 1989; Jasmin et al., 1997). Numerous studies have shown, however, that CeA neurons are physiologically, genetically, and functionally heterogenous (Amano et al., 2012; Chieng et al., 2006; Dumont et al., 2002; Lopez de Armentia and Sah, 2004; Martina et al., 1999; Schiess et al., 1999). To determine which neurons, among this highly heterogeneous group of cells, modulate pain-related behaviors, we took a genetic approach in which we fluorescently labeled molecularly distinct CeA neurons (Figure 1C) (Han et al., 2015; Haubensak et al., 2010; Li et al., 2013) and combined this with optogenetically assisted circuit mapping in acute brain slices or immunohistochemical monitoring of the activated form of the extracellular signal regulated kinase (pERK) or the protein product of the immediate early gene *c-fos* as surrogate markers of neuronal activity. We focused our experiments on CeA-PKCδ and CeA-Som cells because together they constitute the majority of CeA neurons and represent largely nonoverlapping populations (Kim et al., 2017; Li et al., 2013) (Figures S1B and S1C).

To determine if nociceptive inputs from the PB selectively target specific subpopulations of CeA cells, an adeno-associated virus (AAV) encoding channelrhodopsin-2 (AAV-hChR2-EYFP) (Zhao et al., 2011) was stereotaxically injected into the lateral PB of *Prkcd*-Cre::Ai9 or *Sst*-Cre::Ai9 mice (Figure 1D), which allowed us to optogenetically stimulate PB terminals in the CeA (Figure 1E). ChR2-YFP-labeled PB axonal terminals were readily observed within the CeA of PB-injected mice, confirming the efferent projections from the PB to the CeA (Figure 1D). Whole-cell voltage-clamp recordings were obtained from fluorescently labeled CeA-PKCδ or CeA-Som neurons in acute amygdala slices from PB-injected mice. Photostimulation of PB terminals in the CeA with blue light reliably evoked excitatory postsynaptic currents (EPSCs) in most of the neurons recorded (Figure 1F; Table S1), demonstrating that both CeA-PKCδ and CeA-Som neurons receive excitatory inputs from the PB. Immunohistochemical monitoring of cuff-induced pERK or c-Fos further shows that cuff implantation on the sciatic nerve provoked robust ERK activation and c-Fos expression in CeA neurons (Figure S2). Importantly, as illustrated in Figure 2, cuff-induced ERK activation and c-Fos expression were predominantly induced in CeA-PKCδ cells, with minimal (<5%) colocalization between pERK immunofluorescent and Som-tdTomato labeling (Figure 2A) and a much lower (<20%) colocalization between c-Fos and Som-

tdTomato labeling than between c-Fos and PKCδ-tdTomato (Figure 2B). These results demonstrate that molecular changes in CeA-PKCδ neurons correlate with cuff-induced hypersensitivity to cold, heat, tactile, and pinch stimulation, suggesting that CeA-PKCδ neurons may be preferentially recruited and/or sensitized in neuropathic pain conditions.

Nerve Injury Increases the Excitability of CeA-PKCδ Neurons

Sensitization of CeA neurons, manifested as increases in firing rates in response to peripheral stimulation *in vivo* or depolarizing current injections *ex vivo*, in acute brain slices has been reported in various rodent models of persistent pain and shown to be dependent on ERK activation (Han and Neugebauer, 2004; Jiang et al., 2014; Li et al., 2011; Neugebauer and Li, 2003; Neugebauer et al., 2003). Based on these findings and the preferential localization of nerve-injury-induced ERK activation and c-Fos expression to CeA-PKCδ neurons (Figure 2), we hypothesized that pain-related increases in excitability are also localized to CeA-PKCδ neurons. To test this hypothesis, we performed patch-clamp electrophysiological recordings in fluorescently labeled CeA-PKCδ cells in acute amygdala slices obtained from cuff or sham *Prkcd*-Cre::Ai9 mice (Figure 3A). Electrophysiological recordings from CeA-PKCδ fluorescently labeled neurons revealed three different firing types in both cuff and sham cells: spontaneous, late-firing (LF), and regular-spiking (RS) neurons (Figure 3C). Similar proportions of the different firing types were found in both cuff and sham conditions, demonstrating that cuff implantation does not affect the firing phenotypes of CeA-PKCδ neurons. Notably, however, analysis of the intrinsic membrane and firing properties of late-firing CeA-PKCδ neurons demonstrated that firing rates in response to prolonged depolarizing current injections of increasing amplitudes were significantly ($p < 0.05$) larger in CeA-PKCδ late-firing neurons from cuff mice compared to those from sham mice (Figure 3D). The increased excitability of PKCδ late-firing neurons from cuff mice was accompanied by increases in input resistance and decreases in rheobase and current threshold for action potential generation (Figures 3D and 3E). Importantly, resting membrane potentials and supratheshold properties were not altered in cuff PKCδ late-firing neurons, suggesting that the increases in excitability are mediated by changes in subthreshold conductances (Figures 3D and 3E; Table S1). The effects of cuff implantation on the neuronal excitability of CeA-PKCδ neurons was restricted to late-firing neurons as both intrinsic and firing membrane properties were indistinguishable in regular-spiking CeA-PKCδ neurons in both cuff and sham conditions (Table S1). Of note, mapping of the recording sites for the spontaneous, regular-spiking, and late-firing CeA-PKCδ cells in cuff and sham conditions demonstrated that the anatomical distribution of these cells is indistinguishable between firing types and between experimental conditions (Figure S3A). Together with the pERK and c-Fos immunohistochemistry, these electrophysiological experiments suggest that hyperexcitability of CeA-PKCδ late-firing cells underlies cuff-induced tactile hypersensitivity.

Chemogenetic Inhibition of CeA-PKCδ Cells Reverses Nerve-Injury-Induced Tactile and Thermal Hypersensitivity

To establish a causal link between the activity of CeA-PKCδ cells and cuff-induced hypersensitivity to cold, heat, and tactile stimulation, we stereotaxically injected a Cre-dependent AAV encoding the inhibitory designer receptors exclusively activated by designer

drugs (G_iDREADD) hM4Di (AAV8-DIO-hM4Di-mCherry) (Krashes et al., 2011) into the CeA of *Prkcd*-Cre mice (Figure 4A). As illustrated in Figures 4B, 4C, and S4A, unilateral stereotaxic injection of AAV8-DIO-hM4Di-mCherry into the CeA results in robust and localized transduction of hM4Di-mCherry in CeA-PKCδ cells. Whole-cell current-clamp recordings from acute amygdala slices prepared from mice expressing hM4Di in the CeA confirmed that bath application of clozapine-N-oxide (CNO; 10 μM), but not bath application of saline control, significantly inhibits neuronal firing in hM4Di-transduced cells (Figure 4D). The effects of selective inhibition of CeA-PKCδ cells on peripheral sensitivity were then measured before and after i.p. injection of CNO (10 mg/kg body weight) in cuff and sham mice (Figures 4F and 4G). These experiments revealed that CNO-mediated chemogenetic inhibition of CeA-PKCδ cells reverses cuff-induced hypersensitivity to cold, heat, and tactile stimulation in the paw ipsilateral to sciatic nerve injury (Figure 4G). Notably, CNO treatment did not affect baseline responses in sham mice or responses in the paw contralateral to nerve injury (Figures S5A and S5B), demonstrating that the effects of silencing CeA-PKCδ neurons are specific to pathological pain states and that basal activity of these cells does not contribute to pain-related behaviors in the absence of injury. The effects of CNO are hM4Di-specific as CNO injection did not affect cuff-induced hypersensitivity in mice transduced with the mCherry control virus (Figure 4G). Similarly, hM4Di expression in the absence of CNO did not reverse cuff-induced hypersensitivity. The selectivity of the CNO effects indicate that previous reports of DREADD-independent effects of CNO do not underlie the reversal of cuff-induced tactile hypersensitivity induced by chemogenetic inhibition of CeA-PKCδ cells (Gomez et al., 2017; Manvich et al., 2018).

Chemogenetic Activation of CeA-PKCδ Cells Is Sufficient to Promote Bilateral Tactile, but Not Thermal, Hypersensitivity in the Absence of Nerve Injury

The combined results from the pERK and c-Fos immunohistochemistry, electrophysiological experiments in acute slices, and the chemogenetic behavioral experiments presented above demonstrate that sensitization of CeA-PKCδ neurons following nerve injury is necessary for peripheral hypersensitivity to cold, heat, and tactile stimulation of the hindpaw in neuropathic pain conditions and, importantly, that there is no tonic modulation of pain-related responses by CeA-PKCδ cells in the absence of injury. The next set of experiments aimed at determining if activation of CeA-PKCδ cells is sufficient to induce hypersensitivity to cold, heat, and tactile stimulation of the hindpaw. To do this, we infused the excitatory DREADD hM3Dq (AAV8-DIO-hM3Dq-mCherry) into the CeA of *Prkcd*-Cre mice and performed the same battery of behavioral tests before and after the intraperitoneal (i.p.) injection of CNO (10 mg/kg body weight) or saline in cuff, sham, and naive mice (Figure 4F). As illustrated in the slice electrophysiological experiments shown in Figure 4E, bath application of CNO, but not bath application of saline control, significantly depolarized and increased neuronal firing in hM3Dq-transduced cells. At the behavioral level, CNO-mediated chemogenetic activation of CeA-PKCδ cells did not affect sensitivity to cold or heat stimuli in either cuff or sham mice but induced a markedly robust hypersensitivity to tactile stimulation of the hindpaw in the absence of nerve injury in both sham and naive mice (Figure 4H). Consistent with previous reports of bilateral modulation of peripheral tactile sensitivity by unilateral amygdala manipulations (Carrasquillo and Gereau, 2008; Ji and Neugebauer, 2009; Kolber et al., 2010; Li et al., 2017), the effects of unilateral

activation of CeA-PKCδ neurons presented here were observed in both the right and left hindpaw (Figure S5C). Behavioral responses after nerve injury were not affected by CNO-mediated activation of CeA-PKCδ neurons, possibly because the mice are already at the maximum measurable level of hyperalgesia.

Together, these results demonstrate that while activity in CeA-PKCδ neurons is necessary for peripheral tactile and thermal hypersensitivity, activation of these cells in the absence of tissue injury is only sufficient to induce tactile, but not thermal, hypersensitivity.

Nerve Injury Decreases the Excitability of CeA-Som Neurons

CeA-Som cells, which constitute approximately half of the neurons within the CeA, are distinct from, but intermingled with, CeA-PKCδ neurons and have been previously shown to contribute to behavioral responses to threat-predicting sensory cues (Fadok et al., 2017; Yu et al., 2016). Given the overlapping emotional impact of a painful stimulus and a threat, it was surprising to find an almost complete lack of cuff-induced pERK labeling in CeA-Som cells (Figure 2A). To investigate whether CeA-Som cells undergo pain-related changes in neuronal activity, we recorded the firing responses of fluorescently labeled CeA-Som cells in acute slices from cuff and sham-treated *Sst*-Cre::Ai9 mice. These experiments revealed that approximately half (54.8%) of the CeA-Som cells are spontaneously active in sham conditions (Figure 5A). However, in contrast to what we observed in the CeA-PKCδ neurons (Figure 3), the proportion of spontaneously active CeA-Som cells in slices from cuff mice is markedly and significantly reduced compared to that in sham mice (Figure 5A). The firing and intrinsic membrane properties of regular-spiking and late-firing CeA-Som cells were largely indistinguishable in cuff and sham conditions, demonstrating that cuff implantation selectively silences a subpopulation of CeA-Som cells (Table S1). As with the CeA-PKCδ neurons, mapping of the recording sites for the spontaneous, regular-spiking, and late-firing CeA-Som cells in cuff and sham conditions revealed that the anatomical distribution of these cells is indistinguishable between firing types and experimental conditions (Figure S3B). These electrophysiological experiments demonstrate decreases in excitability in CeA cells in the context of persistent pathological pain and, together with the results described above, demonstrate bidirectional cell-type-specific pain-related changes in the excitability of CeA neurons, with CeA-PKCδ cells displaying hyperexcitability and CeA-Som cells displaying hypoexcitability.

CeA-Som Neurons and CeA-PKCδ Cells Bidirectionally Modulate Tactile Sensitivity in Complete Opposite Directions

To establish whether a causal relationship between the hypoexcitability phenotype of CeA-Som cells and peripheral hypersensitivity to thermal and tactile stimuli exists, we stereotaxically injected AAV8-DIO-hM4Di-mCherry (or AAV8-DIO-mCherry) into the CeA of $Sst^{IRES\text{-}Cre}$ mice and measured their responses to cold, heat, and tactile stimulation of the hindpaw before and after the i.p. injection of CNO or saline in cuff, sham, and naive mice (Figure 5F). As illustrated in Figures 5B and S4C, unilateral stereotaxic injection of AAV8-DIO-hM4Di-mCherry into the CeA results in robust and localized transduction of hM4Di-mCherry in CeA-Som cells and reduced firing responses when CNO (10 μM), but not saline, was bath applied (Figure 5D). The effects of selective inhibition of CeA-Som cells on

sensitivity to heat, cold, and tactile stimulation were then measured in both hindpaws before and after i.p. injection of CNO (10 mg/kg body weight) or saline (Figure 5G). In contrast to the antihyperalgesic effects we saw following chemogenetic inhibition of CeA-PKCδ cells after nerve injury and the lack of effects of silencing the CeA-PKCδ cells at baseline conditions (Figure 4F), chemogenetic inhibition of CeA-Som induced tactile hypersensitivity, manifested as a significant ($p < 0.001$) decrease in paw withdrawal thresholds in the absence of tissue injury, in both sham and naive mice (Figure 5G). Notably, responses to heat and cold stimulation are not altered by inhibition of CeA-Som neurons in cuff or sham mice, demonstrating that modulation of nociceptive responses by CeA-Som cells is modality specific. It is also important to note that, in contrast to the anti-hyperalgesic effects of chemogenetic inhibition of CeA-PKCδ neurons in the context of nerve injury (Figure 4G), CNO-mediated inhibition of CeA-Som neurons did not affect behavioral responses after nerve injury (Figure 5G). These results demonstrate that reversal of nerve-injury-induced hypersensitivity is specific to the inhibition of CeA-PKCδ neurons and not mediated by the inhibition of other cell types in the CeA. The lack of enhancement of tactile hypersensitivity in cuff mice might reflect a ceiling effect of measurable hyperalgesia in this model.

Together, the results from these behavioral experiments demonstrate that basal activity of CeA-Som neurons contributes to an endogenous, modality-specific, antinociceptive tone. Similar to the effects of unilateral activation of CeA-PKCδ neurons, the effects of unilateral silencing of CeA-Som neurons are also observed in both the right and left hindpaw (Figures S6A and S6B), demonstrating that inhibition of CeA-Som cells is sufficient to induce tactile hypersensitivity in the absence of nerve injury.

Our electrophysiological experiments demonstrate that nerve injury attenuates the excitability of CeA-Som cells. Based on these findings, we predicted that chemogenetic activation of CeA-Som cells would reverse hypersensitivity in the context of nerve injury. To test this hypothesis, AAV8-DIO-hM3Dq-mCherry was injected into the CeA of *Sst*$^{\text{IRES-Cre}}$ mice, and the effects of i.p. injections of CNO or saline on nerve-injury-induced cold, heat, and tactile hypersensitivity were measured Figure 5F). As illustrated in Figure 5H, chemogenetic activation of CeA-Som cells results in robust analgesia that specifically reverses tactile, but not thermal, nerve-injury-induced hypersensitivity. Notably, chemogenetic activation of CeA-Som neurons did not alter baseline responses to tactile stimulation or responses in the untreated paw (Figure S6C), demonstrating that the contribution of these cells to pain-related behaviors is specific to pathological pain states.

Together, the results presented here demonstrate that the excitability of CeA-Som and CeA-PKCδ cells is differentially influenced by nerve injury and that these cell populations have opposing functions in the modulation of pain-related behaviors, with CeA-Som cells driving hypoalgesia and CeA-PKCδ cells driving hyperalgesia.

DISCUSSION

Previous studies have shown that the CeA is an important site for pain modulation (Neugebauer, 2015; Thompson and Neugebauer, 2017; Veinante et al., 2013). The results

from these reports, however, are contradicting, with some studies demonstrating that the CeA promotes hypersensitivity (Carrasquillo and Gereau, 2007; Kim et al., 2017; Neugebauer et al., 2004) and other studies showing that it promotes analgesia (Fox and Sorenson, 1994; Manning, 1998; Manning et al., 2003; Manning and Mayer, 1995a; b; Manning et al., 2001). Here, we demonstrated that the CeA has a dual function in the modulation of pain, amplifying and attenuating pain-related behaviors in mice. Our study further demonstrated that the direction of pain modulation in the CeA is mediated via opposing changes in the excitability of two major subpopulations of CeA cells, the CeA-PKCδ and CeA-Som neurons. We propose that the CeA functions as a pain rheostat system that enhances or suppresses pain responses under both normal and pathological states (Figure 6).

Dual and Opposing Modulation of Pain-Related Behaviors in the CeA

Maladaptive changes in neuronal excitability and synaptic strength in the CeA underlie persistent pathological pain states. Accordingly, patch-clamp electrophysiological experiments in acute amygdala slices have shown persistent pain-induced increases in the excitability of CeA neurons (Han and Neugebauer, 2004; Jiang et al., 2014; Neugebauer et al., 2003). Consistent with these studies, the results of our study showed pain-related alterations in the excitability of CeA cells, including increases in excitability. Importantly, however, our experiments also revealed that pain-induced changes in excitability in the CeA are bidirectional and cell-type specific. Thus, both increases and decreases in excitability were observed in CeA neurons in the context of pain, with the increases in excitability restricted to CeA neurons that express PKCδ (Figure 4) and the decreases restricted to those expressing somatostatin (Figure 5A).

The decreases in excitability were particularly surprising given that we also show that these cells receive excitatory inputs from the PB and because previous studies have only reported increases in the excitability of CeA neurons in the context of persistent pain. The lack of pain-induced decreases in excitability in previous reports might, therefore, reflect a diluted or masking effect of the phenotype due to previous recordings having been obtained from unidentified populations of CeA cells (Han and Neugebauer, 2004; Neugebauer and Li, 2003; Neugebauer et al., 2003).

Our findings demonstrating that both CeA-PKCδ and CeA-Som neurons are recipients of excitatory inputs from the PB (Figures 1D–1F) are interesting given that our excitability experiments demonstrate cell-type-specific opposing changes in the excitability of these cells following nerve injury (Figures 3 and 5A). Together, these results suggest that changes in the output of these cells, rather than the inputs, are the main driving source of pain-related plasticity. Previous studies have mainly focused on plasticity of synaptic transmission in the CeA as a mechanism underlying behavioral outputs (Ressler and Maren, 2019). Our results demonstrating that cell-type-specific plasticity of intrinsic excitability in the CeA, and not synaptic inputs from the PB to the CeA, underlies pain behavioral sensitization offer an insightful perspective that will be important to consider in future studies evaluating the mechanisms underlying modulation of behavioral outputs in the CeA.

The CeA functions to modulate evolutionarily conserved behavioral responses such as innate and learned responses to threat in a cell-type- and circuit-specific manner (Fadok et al., 2017; Han et al., 2015; Penzo et al., 2014, 2015; Sanford et al., 2017; Yu et al., 2016). Future studies that evaluate the contribution of distinct CeA cell types and circuits to the interactions among fear, stress, context, and pain will be essential for a holistic understanding of the mechanisms underlying modulation of behavioral outputs in the CeA. Previous studies have shown, for example, that CeA-Som cells are activated by threat-predicting cues and drive passive fear responses (Li et al., 2013; Yu et al., 2016). Our results showing that chemogenetic activation of these cells promotes analgesia raises the interesting question of whether activation of CeA-Som cells will underlie fear- and/or stress-induced analgesia. Similar convergence of function might occur in CeA-PKCδ neurons that promote hypersensitivity. Previous studies have shown that optogenetic activation of these cells produces real-time aversion (Yu et al., 2017), predicting that endogenous activation of CeA-PKCδ neurons after injury underlies pain-induced aversion.

Pain ON and OFF Cells

Opposing changes in excitability within a brain region in the context of pain has been previously described in the rostroventromedial medulla (RVM) of rodents with *in vivo* electrophysiological experiments (Fields et al., 1983). These studies described a population of RVM ON cells that display bursts in activity in response to peripheral noxious stimulation just prior to the withdrawal reflex and a second population of RVM cells, the RVM OFF cells, that pause firing responses before the withdrawal reflex when noxious stimuli are peripherally applied. ON and OFF cells with similar electrophysiological responses to peripheral noxious stimuli have also been described in the periaqueductal gray (PAG) and the dorsolateral pontine tegmentum (DLPT) (Haws et al., 1989; Heinricher et al., 1987). While not classically described as ON and OFF cells, neurons that pause or increase firing in response to peripheral noxious stimuli have also been found in *in vivo* recordings of the CeA (Bernard et al., 1992; Neugebauer and Li, 2002). Whether CeA-PKCδ cells and CeA-Som cells display electrophysiological responses *in vivo* that are similar to those described by Fields et al. in the RVM, PAG, and DLPT and, more importantly, whether they undergo pain-induced sensitization in models of persistent pathological pain are important questions for future studies. Based on the results presented here, we predict that the neurons that display increased firing responses to peripheral noxious stimulation *in vivo* are CeA-PKCδ and that those that display inhibition are the CeA-Som neurons.

Modulation of Injury-Induced Hypersensitivity by CeA-PKCδ and CeA-Som Neurons Is Modality Specific

Our experiments demonstrate that modulation of baseline peripheral sensitivity and injury-induced hypersensitivity by CeA-Som and CeA-PKCδ neurons is modality specific. While activity in CeA-PKCδ neurons is required for cold, heat, and tactile hypersensitivity (Figure 4G), activity in these cells in the absence of injury is sufficient to induce only tactile (but not heat or cold) hypersensitivity (Figure 4H). The CeA-Som cells, in contrast, only modulate tactile hypersensitivity (Figures 5G and 5H). Previous studies have found that global manipulations in the CeA do not affect heat hypersensitivity (Carrasquillo and Gereau, 2007), despite the *in vivo* studies demonstrating that a subpopulation of CeA neurons do

respond to heat noxious stimuli (Bernard et al., 1992; Neugebauer and Li, 2002). Our experiments suggest that the heat-responsive neurons in the CeA are the CeA-PKCδ. Our results further support the prediction that distinct input and output profiles of CeA-Som and CeA-PKCδ neurons underlie their opposing functions in the modulation of pain-related behaviors.

Heterogeneity of Function within Genetically Distinct Groups of CeA Neurons

Several studies demonstrate that modulation of behaviors in the CeA is cell-type specific, with many studies focusing on the function of genetically distinct cells (Janak and Tye, 2015; Kim et al., 2017). The results presented here support this idea, demonstrating opposing modulation of pain-related behaviors by two nonoverlapping and genetically distinct subpopulations of CeA cells. A recent study demonstrated, however, that modulation of fear-related behaviors by genetically distinct CeA cells are anatomically segregated (Kim et al., 2017). Thus, CeA-PKCδ neurons that reside in the capsular subdivision of the CeA (CeC) were shown to be functionally opposed to those residing in the lateral subdivision of the CeA (CeL). Results in the present study demonstrate, however, that pain-induced ERK activation and c-Fos expression are localized to both the CeC and CeL (Figure 2). In addition, the anatomical distribution of the late-firing CeA-PKCδ cells that exhibit pain-related increases in excitability is also localized to both the CeC and CeL (Figure S1B). Our results therefore suggest that, in contrast to the CeA-PKCδ cells that modulate fear-related behaviors, the CeA-PKCδ neurons that modulate pain-related behaviors are not anatomically segregated but are instead distributed throughout the CeC and CeL. Consistent with our results, previous studies have shown that, like the CeA-PKCδ cells that modulate pain, the nociceptive inputs from the PB are also localized to both the CeC and CeL (Dong et al., 2010; Sarhan et al., 2005; Sugimura et al., 2016).

It is worthwhile to note, however, that while we did not find anatomical segregation of function within the CeA-PKCδ cells in the context of pain, our results did demonstrate that the electrophysiological properties of these cells are highly heterogenous and that pain-related changes in intrinsic excitability are restricted to late-firing, but not regular-spiking, cells (Figure 3; Table S1). Similarly, the firing types within the CeA-Som cells were also heterogeneous, and while the number of spontaneously active CeA-Som neurons decreased following nerve injury (Figure 5A), the firing properties of all other CeA-Som cell types were unchanged (Table S1).

Together, our findings demonstrate segregation of function within genetically distinct neurons in the modulation of CeA-dependent behaviors that is defined by the firing phenotypes of subpopulations of neurons within these genetically distinct cells. Given that firing phenotypes are tightly regulated by anatomical inputs and the specific repertoire of ion channels expressed, defining the source of the electrophysiological heterogeneity of genetically distinct CeA cells will be an important step forward in our understanding of the mechanisms underlying CeA-dependent behaviors.

The activated form of ERK (pERK) and c-Fos have both been widely used as surrogate markers of neuronal activity, with no consensus in the field as to which is a better marker of injury-induced sensitization (Gao and Ji, 2009). In the present study, we used both markers

to demonstrate that pain-related changes in neuronal activity are preferentially localized to CeA-PKCδ neurons. Activation of ERK in the CeA has been shown to be required for and sufficient to induce behavioral hypersensitivity in several rodent models of pathological pain, including inflammatory (Carrasquillo and Gereau, 2007, 2008; Fu et al., 2008), visceral (Crock et al., 2012; Kim et al., 2010; Sadler et al., 2017), and muscle pain (Cheng et al., 2011; Min et al., 2011).

Previous studies have also characterized the signaling pathways that are upstream and downstream of the activation of ERK in the CeA, further demonstrating the functional contribution of this kinase to the modulation of pain (Cheng et al., 2011; Fu et al., 2008; Kolber et al., 2010; Li et al., 2011; Min et al., 2011). The activation of ERK in all previous studies has been shown to be restricted to a subpopulation of CeA cells that are anatomically localized to the capsular and lateral subdivisions of the CeA. The present study expands our understanding of CeA modulation of pain-related behaviors by demonstrating that ERK activation is largely restricted to CeA-PKCδ neurons, which also show increases in neuronal excitability.

Proposed Model for CeA Modulation of Pain

Our findings demonstrate that two subpopulations of CeA neurons, defined by the expression of either PKCδ or somatostatin, have opposing electrophysiological responses to nerve injury as well as opposing functions in the modulation of pain-related behaviors (Figure 6). These results uncovered a previously unknown causal link between the firing responses of distinct CeA cell types and pain-related behavioral outputs. These results also highlight the functional heterogeneity and complexity of CeA circuits in the modulation of pain. Based on our findings demonstrating that excitability in CeA-PKCδ neurons is increased following injury but that it is attenuated in CeA-Som neurons, we propose a model where the gain of nociceptive inputs to the CeA is increased due to the increased output of CeA-PKCδ neurons in the context of pain. The decreased rheo-base and increased input resistance observed in CeA-PKCδ neurons following nerve injury suggests that changes in subthreshold ionic conductances contribute to the pain-induced hyperexcitability phenotype. This hypothesis, however, does not preclude the possibility that injury-induced sensitization of CeA-PKCδ neurons might also be synaptically driven. Additional experiments are required to dissect out the mechanism driving the injury-induced sensitization of CeA-PKCδ neurons.

Finally, the sources of inhibition of the CeA-Som cells in the context of pathological pain remains unknown. Previous studies have shown, however, that CeA-PKCδ and CeA-Som neurons are synaptically interconnected and can inhibit each other (Ciocchi et al., 2010; Haubensak et al., 2010; Hunt et al., 2017; Li et al., 2013). Based on those results and the present findings, we hypothesize that inhibition of CeA-Som neurons is driven by local inhibitory inputs from the sensitized CeA-PKCδ cells. Determining if nerve-injury-induced strengthening of these synapses is cell-type specific and whether inhibition of CeA-Som cells is downstream or independent of the activation of CeA-PKCδ cells are important questions for future investigations. It will be equally valuable to define the anatomical inputs

and outputs that mediate the opposing function of these CeA cells in the modulation of pain-related behaviors.

STAR★METHODS

LEAD CONTACT AND MATERIALS AVAILABILITY

Further information and requests for resources and reagents should be directed to and will be fulfilled by the Lead Contact, Yarimar Carrasquillo (yarimar.carrasquillo@nih.gov). This study did not generate new unique reagents.

EXPERIMENTAL MODEL AND SUBJECT DETAILS

Mice—Experiments were performed in accordance with the guidelines of the National Institutes of Health (NIH) and were approved by the Animal Care and Use Committee of the National Institute of Neurological Disorders and Stroke and the National Institute on Deafness and other Communication Disorders. Adult (8- to 17-week-old) male mice were used for all experiments, with littermates randomly assigned to experimental groups. Heterozygous male or female *Prkcd*-cre mice (GENSAT – founder line 011559-UCD) were crossed with Swiss-Webster mice (Taconic Farms) or Ai9 mice (Jackson Laboratories); heterozygous male *Sst*-cre (Jackson Laboratory – founder line 018973) were crossed with female C57BL/6NJ (Jackson Laboratory) or Ai9 (Jackson Laboratory) mice; C57BL/6NJ (Jackson Laboratory) were bred as homozygous. Offspring mice were genotyped for the presence of cre-recombinase using DNA extracted from tail biopsies and PCR (Transnetyx) with the following primers: TTAATCCATATTGGCAGAACGAAAACG (forward) and CAGGCTAAGTGCCTTCTCTACA (reverse). Mice were initially housed in groups (up to 5 mice per cage) with their littermates under reversed 12 h light/dark cycle (9 pm to 9 am light). Mice were moved to clean home cages and were housed in pairs, separated by a perforated Plexiglas divider following surgeries. Food and water were provided *ad libitum*. One week prior to behavioral, electrophysiological or histological experiments, mice were handled by the experimenter for 5 min and received a mock intraperitoneal (i.p.) injection (0.1 mL of sterile saline) daily.

METHOD DETAILS

Viral vectors—AAV8-hSyn-DIO-hM4Di-mCherry (Addgene viral prep # 44362-AAV8) (Krashes et al., 2011), AAV8-hSyn-DIO-mCherry (Addgene viral prep # 50459-AAV8), pAAV-hSyn-DIO-hM3D(Gq)-mCherry (Addgene viral prep #44361-AAV8) and AAV2-hsyn-hChR2(H134R)-EYFP (UNC Vector Core, Lot Number AV4384G) (Zhao et al., 2011), were produced by Addgene and the Vector Core at the University of North Carolina and stored in aliquots at −80°C until use.

Surgical procedures

Stereotaxic intra-amygdala injections: Acute microinjections were performed as previously described using a Model 940 small animal stereotaxic instrument (David Kopf Instruments) (Carrasquillo and Gereau, 2007). Mice were deeply anesthetized with 2% isoflurane at a flow rate of 0.5 L/min and micro-injected with AAV8-hSyn-DIO-hM4Di-mCherry, AAV8-hSyn-DIO-mCherry or AAV8-hSyn-DIO-hM3Dq-mcherry into the right

CeA or LPB using a Hamilton 0.5 μl syringe including a 32-gauge needle (Neuro model 7000.5 KH). The right CeA was selected because previous reports have shown right hemisphere lateralization of amygdala function in the modulation of tactile hypersensitivity in mice (Carrasquillo and Gereau, 2008; Ji and Neugebauer, 2009; Kolber et al., 2010; Li et al., 2017). A total volume of 0.03 μl was injected in *Sst*-cre mice; 0.3 μl was injected in *Prkcd*-cre mice. Injections were performed at a flow rate of 0.1 μl/min and the injector was left in place at the end of the injection for an additional 15 min after to allow for virus diffusion. The following stereotaxic coordinates were used to target the CeA in *Prkcd*-cre mice: 1.4 mm posterior from bregma, 3.2 mm lateral to midline, 4.8 mm ventral to skull surface. The stereotaxic coordinates for *Sst*-cre mice were: 1.25 mm posterior from bregma, 3.0 mm lateral to midline, 4.5 mm ventral to skull surface. Lateral parabrachial nucleus injections were performed as described above. A total volume of 0.1 μl was injected in *Prkcd*-cre mice using the following stereotaxic coordinates: 5.0 mm posterior from bregma, 1.30 mm lateral to midline, 3.52 mm ventral to skull surface. A total volume of 0.1 μl was injected in *Sst*-cre mice using the following stereotaxic coordinates: 4.9 mm posterior from bregma, 1.2 mm lateral to midline, 3.78 mm ventral to skull surface. Mice recovered for 1 week before additional experimental procedures. At the end of each experiment, mice were transcardially perfused with 4% paraformaldehyde solution in 0.1 M Phosphate Buffer (PFA/PB), pH 7.4 and the brains were stained for mCherry as described below to verify injection site. Anatomical limits of each region were identified using a mouse brain atlas (Paxinos and Franklin, 2001) and drawings of the virus spread as a function of the rostro-caudal level were performed for each injected mouse. Only mice that had virus injection restricted to the CeA were used for behavioral experiments.

Sciatic cuff implantation: Sciatic nerve surgeries were performed as previously described (Benbouzid et al., 2008). Mice were anesthetized with 2% isoflurane at a flow rate of 0.5 L/min and a 1-cm long incision was made in the proximal one third of the lateral thigh. The sciatic nerve was exteriorized with forceps inserted under the nerve and gently stretched using the forceps. A 2 mm-long-piece of PE-20 non-toxic, sterile polyethylene tubing (0.38 mm ID / 1.09 mm OD; Daigger Scientific) split along its side was slid onto the exposed part of the sciatic nerve. For sham mice, the sciatic nerve was exteriorized and gently stretched using forceps and then returned to its normal position. The skin was closed with wound clips following each surgery. All testing in these mice occurred 1 week after recovery from surgery.

Nociceptive testing—All behavioral testing was performed during the dark phase, under red light, by an experimenter blinded to treatment. For all chemogenetic experiments, clozapine-N-oxide (CNO; Enzo Life Sciences) was injected i.p. (10 mg/kg body weight) 45 min to 1 h before testing.

Von Frey Filaments Test: Mice were habituated (for 3 h) and tested in 11 × 11 × 13 cm ventilated opaque white Plexiglas boxes placed on an elevated mesh platform. Mechanical sensitivity was measured by a female experimenter using von Frey filaments (North Coast Medical, Inc. San Jose, CA) as previously described (Carrasquillo and Gereau, 2007). Each von Frey filament, starting with the smallest, was applied to the mouse hindpaw until bent at

30° for ~2 s. The smallest filament that evoked a paw withdrawal response in at least three of five trials was taken as the mechanical threshold for that trial. Three to five baseline measurements were taken from each hindpaw before surgery and 1 week after cuff/sham surgery. The average was calculated individually for each paw. Mechanical hypersensitivity was assessed by comparing withdrawal thresholds before and after cuff, sham or drug treatment.

Randall-Selitto Test: Response thresholds to mechanical pressure stimulation (pinch) of the hindpaws were measured by a female experimenter using a modified version of the Randall-Selitto test as previously described (Randall and Selitto, 1957). Mice were briefly anesthetized in 3% isoflurane in an induction chamber, then kept lightly anesthetized with 0.5%–1% isoflurane at a flow rate of 0.5 L/min. A sharp pinch, not exceeding 200 g of force, was delivered to the plantar surface of the hindpaw ipsilateral to sciatic nerve treatment. Pinch pressure that elicited withdrawal was recorded at 1minute intervals for 30 minutes. The average was calculated individually for each animal.

Hargreaves Test: Assessment of thermal sensitivity in cuff and sham mice was performed by a male experimenter using a modified version of the Hargreaves test (Hargreaves et al., 1988) as described previously (Carrasquillo and Gereau, 2007). Mice were tested in ventilated opaque white Plexiglas testing chambers (11 × 11 × 13 cm) placed on an elevated platform with a clear glass surface heated to 30°C. Following a 1 h period of habituation, a thermal stimulus from a constant radiant heat source (active intensity of 25 for C57BL/6NJ and 35 for Swiss-Webster background mice) was delivered through the glass bottom of the chamber to the plantar surface of the hindpaw (IITC Life Sciences, Woodland Hills, CA). The time to paw withdrawal was recorded. The average of five latencies were taken from each hindpaw before, 1 and 24 hours after drug treatment.

Acetone Evaporative Test: The acetone evaporative test (Choi et al., 1994) was adapted to measure sensitivity to a cold stimulus and was performed by a male experimenter. Cuff and sham mice were placed for habituation in a ventilated opaque white Plexiglas testing chamber (11 × 11 × 13 cm) on an elevated metal wire for 3 hours. Acetone (Sigma) was drawn into a 1 mL syringe and a drop was lightly applied through the wire mesh to the plantar surface of the hindpaw, being careful not to directly touch the paw with the syringe to avoid false withdrawal responses. Following acetone application, nociceptive responses were quantified for 60 s using a modified version of the scoring system described previously (Colburn et al., 2007) where 0 = a rapid transient lifting, licking, or shaking of the hindpaw, which subsides immediately; 1 = lifting, licking, and/or shaking of the hindpaw, which continues beyond the initial application, but subsides within 5 s; 2 = protracted, repeated lifting, licking, and/or shaking of the hindpaw. The average score of five stimulations were taken from each hindpaw before, 1 and 24 hours after drug treatment.

Immunohistochemistry—At the end of each experiment, mice were deeply anesthetized with 1.25% Avertin anesthesia (2,2,2-tribromoethanol and tert-amyl alcohol in 0.9% NaCl; 0.025 ml/g body weight), then perfused transcardially with 0.9% NaCl (37°C), followed by 100 mL of ice-cold 4% PFA/PB. For the c-Fos experiments, mice were euthanized 1h after

the completion of the Randall-Selitto test. The brain was dissected and postfixed in 4% PFA/PB overnight at 4°C. After cryoprotection in 30% sucrose/PB for 48 h, coronal sections (30 μm) were obtained using a freezing sliding microtome and stored in 0.1 M Phosphate Buffered Saline (PBS), pH 7.4 containing 0.01% sodium azide (Sigma) at 4°C until immunostaining. Sections were rinsed in PBS, incubated in 0.1% Triton X-100 in PBS for 10 minutes at room temperature and blocked in 5% normal goat serum (NGS) (Vector Labs, Burlingame, CA) with 0.1% Triton X-100, 0.05% Tween-20 and 1% bovine serum albumin (BSA) for 30 minutes at room temperature. Sections were then incubated for 72 h at 4°C in rat anti-mCherry (1:500, Invitrogen, M11217), rabbit anti-Phospho-p44/42 MAPK (Erk1/2) (1:200, Cell Signaling Technology, 9101L), rabbit anti-Phospho-c-Fos (Ser32) (1:2000, Cell Signaling Technology, #5348), rabbit anti-GFP (1:500, Invitrogen, A6455) and/or mouse anti-PKCδ (1:1000, BD Biosciences, 610397) in 1.5% NGS blocking solution with 0.1% Triton X-100, 0.05% Tween-20 and 1% BSA. Sections were then rinsed in PBS and incubated in goat anti-rat Cy3 (1:250, Invitrogen, A10522), Alexa Fluor 647-conjugated goat anti-rabbit (1:100, Invitrogen, A21244), goat anti-Rabbit IgG (H+L) Highly Cross-Adsorbed Secondary Antibody, Alexa Fluor 488 (1:200, Invitrogen, A-11034) and/or Alexa Fluor 647-conjugated goat anti-mouse (1:100, Invitrogen, A21235) secondary antibodies in 1.5% NGS blocking solution with 0.1% Triton X-100, 0.05% Tween 20 and 1% BSA, protected from light, for 2 h at room temperature. Sections were then rinsed in PBS, mounted on positively charged glass slides, air-dried and coverslips were placed using Fluoromount-G (SouthernBiotech).

Image acquisition and analysis—Image acquisition was performed using a Nikon A1R laser scanning confocal microscope and a 2× (for low magnification) or a 20× (for high magnification) objective. Representative high magnification images were collected using a 40× oil-immersion objective. All image analyses were performed from the images collected using the 20× objective and with the experimenter blinded to experimental group. Laser intensity, gain, and pinhole were kept constant between experiments. Sequential acquisition of multiple channels was used, and z stacks were collected at 0.9 μm steps. Images were collected at a size of 0.7 × 0.59 mm and were automatically stitched upon acquisition using NIS Elements software. Image stacks were converted into maximum intensity z-projections using the NIS Elements software. Quantitative analysis was performed in the CeA, between bregmas −0.58 and −1.94. Anatomical limits of each region were identified using a mouse brain atlas (Paxinos and Franklin, 2001). Quantification of the number of positive cells was performed manually for each channel using the software NIS Elements and were quantified using 1 section per rostrocaudal level per mouse. Co-labeled cells were automatically identified by NIS Elements software and were visually corroborated by an experimenter.

Ex-vivo electrophysiology

Preparation of acute amygdala slices: Slices were prepared from brains of (9-to 17-week-old) mice using standard procedures (Davie et al., 2006) 1-2 weeks after cuff or sham surgery, 2-3 weeks after AAV8-hSyn-DIO-hM4D$_i$-mCherry or AAV8-hSyn-DIO-mCherry injection into the CeA, or 5-6 weeks after AAV2-hsyn-hChR2(H134R)-EYFP injection into the PB. Briefly, mice were deeply anesthetized with 1.25% Avertin anesthesia (0.025 ml/g of body weight and then perfused transcardially with ice-cold cutting solution containing (in

mM): 110.0 choline chloride, 25.0 $NaHCO_3$, 1.25 NaH_2PO_4, 2.5 KCl, 0.5 $CaCl_2$, 7.2 $MgCl_2$, 25 D-glucose, 12.7 L-ascorbic acid, 3.1 pyruvic acid, and saturated with 95% O_2—5% CO_2. Brains were rapidly removed and placed in ice-cold cutting solution. Coronal slices (250-300 μm) containing the central amygdala were cut on a Leica VT1200 S vibrating blade microtome (Leica Microsystems Inc., Buffalo Grove, IL, USA) and incubated in a holding chamber with oxygenated artificial cerebral spinal fluid (ACSF) containing (in mM): 125 NaCl, 2.5 KCl, 1.25 NaH_2PO_4, 25 $NaHCO_3$, 2.0 $CaCl_2$, 1.0 $MgCl_2$, 25 D-glucose (~310 $mosmol^{-1}$), saturated with 95% O_2—5% CO_2, at 33°C for 30 minutes, then moved to room temperature for at least an additional 20 minutes before transfer to the recording chamber.

Electrophysiological Recording: Electrophysiological experiments were performed blind to experimental treatment. Whole-cell current-clamp and voltage-clamp recordings were obtained at 33 ± 1°C from visually identified tdTomato-expressing CeA neurons using differential interference contrast optics with infrared illumination. Recording electrodes were positioned in the CeA under visual control. The CeA was identified based on the distinctive fiber bundles that clearly delineate its structure. For current-clamp experiments, slices were perfused continuously with ACSF, 95% 0_2—5% CO_2. ACSF (with or without Picrotoxin (100 μM), Tetrodotoxin (1 μM) and/or 4-Aminopyridine (100 μM)) was used for voltage-clamp experiments. Recording pipettes for current-clamp experiments contained a potassium methylsulfate-based internal solution (in mM): 120 $KMeSO_4$, 20 KCl, 10 HEPES, 0.2 EGTA, 8 NaCl, 4 Mg-ATP, 0.3 Tris-GTP, 14 Phosphocreatine, pH 7.3 with KOH (~300 $mosmol^{-1}$). The composition of the internal solution for the voltage-clamp experiments was either cesium gluconate-based (in mM: 120 cesium gluconate, 6 NaCl, 10 HEPES hemisodium, 12 phosphocreatine Na2, 5 EGTA, 1 CaCl2, 2 MgCl2, 2 ATP Mg, and 0.5 GTP Na (pH 7.4 as adjusted with CsOH; osmolarity, approximately 290 mOsm/kg) or potassium methylsulfate-based. Biocytin (3 mg/ml) was added to the solution in some recordings. Pipette resistances were 2-6 MΩ, with series resistances not exceeding 20 MΩ. Experiments were controlled and data was collected using the Multiclamp 700B patch-clamp amplifier interfaced with a Digidata 1550 acquisition system and pCLAMP 10.7 software (Axon Instruments, Union City, CA, USA) to a Dell computer. Tip potentials were zeroed before membrane-pipette seals were formed; pipette capacitances and series resistances were compensated and monitored using the pCLAMP software, throughout recording. Single and repetitive action potential firings were elicited from resting membrane potentials in response to brief (5 ms) and prolonged (500 ms) depolarizing current injections of variable amplitudes, respectively. Spontaneously active neurons were recorded for 5 minutes, gap-free, in the cell-attached configuration, and 1-minute gap-free after break-in. For the optogenetic stimulation experiments, light-evoked excitatory postsynaptic currents were recorded at a holding potential of −60 mV and ChR2 was activated using an LED illumination system (λ = 470 nm, Mightex) controlled by pCLAMP 10.7 software. Light pulses of 5 ms were delivered at 10 Hz to drive synaptic responses. For validation of CNO effects on hM3Dq- and hM4Di-transduced cells, current-clamp recordings were performed with 5 μM CPP (-((R)-2-carboxypiperazin-4-yl)-propyl-1-phosphonic acid), 10 μM NBQX (2,3-dioxo-6-nitro-1,2,3,4-tetrahydrobenzo[f]quinoxaline-7-sulfonamide) and 5 μM GABAzine (6-imino-3-(4-methoxyphenyl)-1(6H)-pyridazinebutanoic acid hydrobromide).

Changes in excitability were measured using a 500 ms current injection that elicited between 3 and 6 action potentials. After at least 10 recordings of stable action potential firing, 10 μM CNO or vehicle in ACSF and synaptic blocker was applied via bath application. The same current injection was used to elicit action potentials throughout bath application. Once the cell began to fire stably, 10 additional recordings were performed. Both the number of elicited spikes and resting membrane potential were analyzed to assess excitability. Values were averaged across five stable traces. For LPB recordings, pipette resistances were 4-7 MΩ, with series resistances not exceeding 40 MΩ. Signals were acquired at 100 kHz and filtered at 10 kHz before digitization and storage.

Data Analysis: Data were compiled and analyzed using ClampFit 10.7 (Molecular Devices), Microsoft Excel, Mini Analysis (v. 6.0.7, Synaptosoft, Inc., Decatur, GA, USA) and Prism (v. 7, GraphPad Software Inc., La Jolla, CA, USA). Input resistances (R_{in}) were calculated from the average change in membrane potential produced by a 20-pA hyperpolarizing and depolarizing current injection from the resting membrane potential. Rheobase was defined as the minimal current that induces an action potential in response to 500-ms depolarizing current injection. Voltage sag (V_{sag}) was calculated as the difference between the steady state voltage and the peak voltage response to a 500-pA hyperpolarizing current injection. The properties (current threshold for action potential generation, amplitudes, voltage thresholds, widths at half-maximum, rise and decay times) of individual action potentials were determined offline using Mini Analysis (version 6.0.7; Synaptosoft). In each cell, action potential amplitude was measured as the voltage difference between the resting membrane potential and the peak of the action potential. The current threshold for action potential generation (I_{thr}) was defined as the minimal current injection, applied (for 5 ms) from the resting membrane potential, required to evoke a single action potential; voltage threshold (V_{thr}) for action potential generation was determined from the third derivative of the variation in the membrane voltage as a function of time (dV/dt) during the rising phase of the action potential. Differentiated traces were filtered with a digital Gaussian filter and smoothed by 100 points to determine V_{thr} (Synaptosoft, Inc.). Width at half-maximum was determined from measurement of the duration of the action potential when the membrane voltage had returned from the peak halfway back to the resting membrane potential. Rise times were determined as the time required for the membrane voltage to reach peak amplitude from V_{thr}. Decay times were determined as the time required for the membrane voltage to decrease from 90% of the peak amplitude to V_{thr}. Drawings depicting the recording site for each cell were made based on the CeA anatomical limits described in the mouse brain atlas (Paxinos and Franklin, 2001).

QUANTIFICATION AND STATISTICAL ANALYSIS

Results are expressed as means ± SEM. Statistical analyses were performed using Student's (unpaired) t test, Chi-square (one-sided) or two-way analysis of variance (ANOVA) followed by Sidak's or Dunnett's multiple comparison tests using GraphPad Prism (v. 7.0). Sample sizes are indicated in the figure legends. All experiments were replicated at least once.

DATA AND CODE AVAILABILITY

All the data presented in this study are available from the corresponding author upon request.

Supplementary Material

Refer to Web version on PubMed Central for supplementary material.

ACKNOWLEDGMENTS

This work was supported by the Intramural Research Program of the National Center for Complementary and Integrative Health, NIH. We thank Allan Basbaum, Mario Penzo, and Yavin Shaham for comments on this manuscript and Gary Soroosh, Jon Macleod, Simón Arango, Yonatan Arnold, Sudhuman Singh, and Jordan Becker for assistance with the immunohistochemical experiments. pAAV-hSyn-DIO-hM3D(Gq)-mCherry (Addgene viral prep # 44361-AAV8), pAAV-hSyn-DIO-hM4D(G_i)-mCherry (Addgene viral prep # 44362-AAV8), and pAAV-hSyn-DIO-mCherry (Addgene viral prep # 50459-AAV8) were a gift from Bryan Roth. The AAV2-hsyn-hChR2(H134R)-EYFP was provided by the Vector Core at the University of North Carolina, with a material transfer agreement with Professor Karl Deisseroth (Stanford University)

REFERENCES

Amano T, Amir A, Goswami S, and Paré D (2012). Morphology, PKCδ expression, and synaptic responsiveness of different types of rat central lateral amygdala neurons. J. Neurophysiol 108, 3196–3205. [PubMed: 22972957]

Benbouzid M, Pallage V, Rajalu M, Waltisperger E, Doridot S, Poisbeau P, Freund-Mercier MJ, and Barrot M (2008). Sciatic nerve cuffing in mice: a model of sustained neuropathic pain. Eur. J. Pain 12, 591–599. [PubMed: 18006342]

Bernard JF, and Besson JM (1990). The spino(trigemino)pontoamygdaloid pathway: electrophysiological evidence for an involvement in pain processes. J. Neurophysiol 63, 473–490. [PubMed: 2329357]

Bernard JF, Peschanski M, and Besson JM (1989). A possible spino (trigemino)-ponto-amygdaloid pathway for pain. Neurosci. Lett 100, 83–88. [PubMed: 2474780]

Bernard JF, Huang GF, and Besson JM (1992). Nucleus centralis of the amygdala and the globus pallidus ventralis: electrophysiological evidence for an involvement in pain processes. J. Neurophysiol 68, 551–569. [PubMed: 1527575]

Bourbia N, Ansah OB, and Pertovaara A (2010). Corticotropin-releasing factor in the rat amygdala differentially influences sensory-discriminative and emotional-like pain response in peripheral neuropathy. J. Pain 11, 1461–1471. [PubMed: 20624690]

Bushnell MC, Ceko M, and Low LA (2013). Cognitive and emotional control of pain and its disruption in chronic pain. Nat. Rev. Neurosci 14, 502–511. [PubMed: 23719569]

Carrasquillo Y, and Gereau RW 4th. (2007). Activation of the extracellular signal-regulated kinase in the amygdala modulates pain perception. J. Neurosci 27, 1543–1551. [PubMed: 17301163]

Carrasquillo Y, and Gereau RW 4th. (2008). Hemispheric lateralization of a molecular signal for pain modulation in the amygdala. Mol. Pain 4, 24. [PubMed: 18573207]

Cheng SJ, Chen CC, Yang HW, Chang YT, Bai SW, Chen CC, Yen CT, and Min MY (2011). Role of extracellular signal-regulated kinase in synaptic transmission and plasticity of a nociceptive input on capsular central amygdaloid neurons in normal and acid-induced muscle pain mice. J. Neurosci 31, 2258–2270. [PubMed: 21307262]

Chieng BC, Christie MJ, and Osborne PB (2006). Characterization of neurons in the rat central nucleus of the amygdala: cellular physiology, morphology, and opioid sensitivity. J. Comp. Neurol 497, 910–927. [PubMed: 16802333]

Choi Y, Yoon YW, Na HS, Kim SH, and Chung JM (1994). Behavioral signs of ongoing pain and cold allodynia in a rat model of neuropathic pain. Pain 59, 369–376. [PubMed: 7708411]

Ciocchi S, Herry C, Grenier F, Wolff SB, Letzkus JJ, Vlachos I, Ehrlich I, Sprengel R, Deisseroth K, Stadler MB, et al. (2010). Encoding of conditioned fear in central amygdala inhibitory circuits. Nature 468, 277–282. [PubMed: 21068837]

Colburn RW, Lubin ML, Stone DJ Jr., Wang Y, Lawrence D, D'Andrea MR, Brandt MR, Liu Y, Flores CM, and Qin N (2007). Attenuated cold sensitivity in TRPM8 null mice. Neuron 54, 379–386. [PubMed: 17481392]

Crock LW, Kolber BJ, Morgan CD, Sadler KE, Vogt SK, Bruchas MR, and Gereau RW 4th. (2012). Central amygdala metabotropic glutamate receptor 5 in the modulation of visceral pain. J. Neurosci 32, 14217–14226. [PubMed: 23055491]

Davie JT, Kole MH, Letzkus JJ, Rancz EA, Spruston N, Stuart GJ, and Hausser M (2006). Dendritic patch-clamp recording. Nat. Protoc 1, 1235–1247. [PubMed: 17406407]

Davis M (1994). The role of the amygdala in emotional learning. Int. Rev. Neurobiol 36, 225–266. [PubMed: 7822117]

Davis M, and Whalen PJ (2001). The amygdala: vigilance and emotion. Mol. Psychiatry 6, 13–34. [PubMed: 11244481]

Dong YL, Fukazawa Y, Wang W, Kamasawa N, and Shigemoto R (2010). Differential postsynaptic compartments in the laterocapsular division of the central nucleus of amygdala for afferents from the parabrachial nucleus and the basolateral nucleus in the rat. J. Comp. Neurol 518, 4771–4791. [PubMed: 20963828]

Dumont EC, Martina M, Samson RD, Drolet G, and Paré D (2002). Physiological properties of central amygdala neurons: species differences. Eur. J. Neurosci 15, 545–552. [PubMed: 11876782]

Fadok JP, Krabbe S, Markovic M, Courtin J, Xu C, Massi L, Botta P, Bylund K, Müller C, Kovacevic A, et al. (2017).A competitive inhibitory circuit for selection of active and passive fear responses. Nature 542, 96–100. [PubMed: 28117439]

Fields HL, Bry J, Hentall I, and Zorman G (1983). The activity of neurons in the rostral medulla of the rat during withdrawal from noxious heat. J. Neurosci 3, 2545–2552. [PubMed: 6317812]

Fox RJ, and Sorenson CA (1994). Bilateral lesions of the amygdala attenuate analgesia induced by diverse environmental challenges. Brain Res. 648, 215–221. [PubMed: 7922536]

Fu Y, Han J, Ishola T, Scerbo M, Adwanikar H, Ramsey C, and Neugebauer V (2008). PKA and ERK, but not PKC, in the amygdala contribute to pain-related synaptic plasticity and behavior. Mol. Pain 4, 26. [PubMed: 18631385]

Gao YJ, and Ji RR (2009). c-Fos and pERK, which is a better marker for neuronal activation and central sensitization after noxious stimulation and tissue injury? Open Pain J. 2, 11–17. [PubMed: 19898681]

Gomez JL, Bonaventura J, Lesniak W, Mathews WB, Sysa-Shah P, Rodriguez LA, Ellis RJ, Richie CT, Harvey BK, Dannals RF, et al. (2017). Chemogenetics revealed: DREADD occupancy and activation via converted clozapine. Science 357, 503–507. [PubMed: 28774929]

Han JS, and Neugebauer V (2004). Synaptic plasticity in the amygdala in a visceral pain model in rats. Neurosci. Lett 361, 254–257. [PubMed: 15135941]

Han S, Soleiman MT, Soden ME, Zweifel LS, and Palmiter RD (2015). Elucidating an affective pain circuit that creates a threat memory. Cell 162, 363–374. [PubMed: 26186190]

Hargreaves K, Dubner R, Brown F, Flores C, and Joris J (1988). A new and sensitive method for measuring thermal nociception in cutaneous hyperalgesia. Pain 32, 77–88. [PubMed: 3340425]

Haubensak W, Kunwar PS, Cai H, Ciocchi S, Wall NR, Ponnusamy R, Biag J, Dong HW, Deisseroth K, Callaway EM, et al. (2010). Genetic dissection of an amygdala microcircuit that gates conditioned fear. Nature 468, 270–276. [PubMed: 21068836]

Haws CM, Williamson AM, and Fields HL (1989). Putative nociceptive modulatory neurons in the dorsolateral pontomesencephalic reticular formation. Brain Res. 483, 272–282. [PubMed: 2706520]

Heinricher MM, Cheng ZF, and Fields HL (1987). Evidence for two classes of nociceptive modulating neurons in the periaqueductal gray. J. Neurosci 7, 271–278. [PubMed: 3806198]

Hunt S, Sun Y, Kucukdereli H, Klein R, and Sah P (2017). Intrinsic circuits in the lateral central amygdala. eNeuro 4, ENEURO.0367-16.2017.

Janak PH, and Tye KM (2015). From circuits to behaviour in the amygdala. Nature 517, 284–292. [PubMed: 25592533]

Jasmin L, Burkey AR, Card JP, and Basbaum AI (1997). Transneuronal labeling of a nociceptive pathway, the spino-(trigemino-)parabrachio-amygdaloid, in the rat. J. Neurosci 17, 3751–3765. [PubMed: 9133395]

Ji G, and Neugebauer V (2009). Hemispheric lateralization of pain processing by amygdala neurons. J. Neurophysiol 102, 2253–2264. [PubMed: 19625541]

Jiang H, Fang D, Kong LY, Jin ZR, Cai J, Kang XJ, Wan Y, and Xing GG (2014). Sensitization of neurons in the central nucleus of the amygdala via the decreased GABAergic inhibition contributes to the development of neuropathic pain-related anxiety-like behaviors in rats. Mol. Brain 7, 72. [PubMed: 25277376]

Kim SH, Han JE, Hwang S, and Oh DH (2010). The expression of corticotropin-releasing factor in the central nucleus of the amygdala, induced by colorectal distension, is attenuated by general anesthesia. J. Korean Med. Sci 25, 1646–1651. [PubMed: 21060755]

Kim J, Zhang X, Muralidhar S, LeBlanc SA, and Tonegawa S (2017). Basolateral to central amygdala neural circuits for appetitive behaviors. Neuron 93, 1464–1479.e1465. [PubMed: 28334609]

Kolber BJ, Montana MC, Carrasquillo Y, Xu J, Heinemann SF, Muglia LJ, and Gereau RW 4th. (2010). Activation of metabotropic glutamate receptor 5 in the amygdala modulates pain-like behavior. J. Neurosci 30, 8203–8213. [PubMed: 20554871]

Krashes MJ, Koda S, Ye C, Rogan SC, Adams AC, Cusher DS, Maratos-Flier E, Roth BL, and Lowell BB (2011). Rapid, reversible activation of AgRP neurons drives feeding behavior in mice. J. Clin. Invest 121, 1424–1428. [PubMed: 21364278]

Li Z, Ji G, and Neugebauer V (2011). Mitochondrial reactive oxygen species are activated by mGluR5 through IP3 and activate ERK and PKA to increase excitability of amygdala neurons and pain behavior. J. Neurosci 31, 1114–1127. [PubMed: 21248136]

Li H, Penzo MA, Taniguchi H, Kopec CD, Huang ZJ, and Li B (2013). Experience-dependent modification of a central amygdala fear circuit. Nat. Neurosci 16, 332–339. [PubMed: 23354330]

Li Z, Yin P, Chen J, Li C, Liu J, Rambojan H, and Luo F (2017). Activation of the extracellular signal-regulated kinase in the amygdale modulates fentanyl-induced hypersensitivity in rats. J. Pain 18, 188–199. [PubMed: 27838497]

Lopez de Armentia M, and Sah P (2004). Firing properties and connectivity of neurons in the rat lateral central nucleus of the amygdala. J. Neurophysiol 92, 1285–1294. [PubMed: 15128752]

Manning BH (1998). A lateralized deficit in morphine antinociception after unilateral inactivation of the central amygdala. J. Neurosci 18, 9453–9470. [PubMed: 9801383]

Manning BH, and Mayer DJ (1995a). The central nucleus of the amygdala contributes to the production of morphine antinociception in the formalin test. Pain 63, 141–152. [PubMed: 8628579]

Manning BH, and Mayer DJ (1995b). The central nucleus of the amygdala contributes to the production of morphine antinociception in the rat tail-flick test. J. Neurosci 15, 8199–8213. [PubMed: 8613754]

Manning BH, Merin NM, Meng ID, and Amaral DG (2001). Reduction in opioid- and cannabinoid-induced antinociception in rhesus monkeys after bilateral lesions of the amygdaloid complex. J. Neurosci 21, 8238–8246. [PubMed: 11588195]

Manning BH, Martin WJ, and Meng ID (2003). The rodent amygdala contributes to the production of cannabinoid-induced antinociception. Neuroscience 120, 1157–1170. [PubMed: 12927220]

Manvich DF, Webster KA, Foster SL, Farrell MS, Ritchie JC, Porter JH, and Weinshenker D (2018). The DREADD agonist clozapine N-oxide (CNO) is reverse-metabolized to clozapine and produces clozapine-like interoceptive stimulus effects in rats and mice. Sci. Rep 8, 3840. [PubMed: 29497149]

Martina M, Royer S, and Paré D (1999). Physiological properties of central medial and central lateral amygdala neurons. J. Neurophysiol 82, 1843–1854. [PubMed: 10515973]

Min MY, Yang HW, Yen CT, Chen CC, Chen CC, and Cheng SJ (2011). ERK, synaptic plasticity and acid-induced muscle pain. Commun. Integr. Biol 4, 394–396. [PubMed: 21966555]

Nahin RL (2015). Estimates of pain prevalence and severity in adults: United States, 2012. J. Pain 16, 769–780. [PubMed: 26028573]

Nation KM, De Felice M, Hernandez PI, Dodick DW, Neugebauer V, Navratilova E, and Porreca F (2018). Lateralized kappa opioid receptor signaling from the amygdala central nucleus promotes stress-induced functional pain. Pain 159, 919–928. [PubMed: 29369967]

Neugebauer V (2015). Amygdala pain mechanisms. Handb. Exp. Pharmacol 227, 261–284. [PubMed: 25846623]

Neugebauer V, and Li W (2002). Processing of nociceptive mechanical and thermal information in central amygdala neurons with knee-joint input. J. Neurophysiol 87, 103–112. [PubMed: 11784733]

Neugebauer V, and Li W (2003). Differential sensitization of amygdala neurons to afferent inputs in a model of arthritic pain. J. Neurophysiol 89, 716–727. [PubMed: 12574449]

Neugebauer V, Li W, Bird GC, Bhave G, and Gereau RW 4th. (2003). Synaptic plasticity in the amygdala in a model of arthritic pain: differential roles of metabotropic glutamate receptors 1 and 5. J. Neurosci 23, 52–63. [PubMed: 12514201]

Neugebauer V, Li W, Bird GC, and Han JS (2004). The amygdala and persistent pain. Neuroscientist 10, 221–234. [PubMed: 15155061]

Paxinos G, and Franklin KBJ (2001). The Mouse Brain in Stereotaxic Coordinates, Second Edition (Academic Press).

Penzo MA, Robert V, and Li B (2014). Fear conditioning potentiates synaptic transmission onto long-range projection neurons in the lateral subdivision of central amygdala. J. Neurosci 34, 2432–2437. [PubMed: 24523533]

Penzo MA, Robert V, Tucciarone J, De Bundel D, Wang M, Van Aelst L, Darvas M, Parada LF, Palmiter RD, He M, et al. (2015). The paraventricular thalamus controls a central amygdala fear circuit. Nature 519, 455–459. [PubMed: 25600269]

Randall LO, and Selitto JJ (1957). A method for measurement of analgesic activity on inflamed tissue. Arch. Int. Pharmacodyn. Ther 111, 409–419. [PubMed: 13471093]

Ressler RL, and Maren S (2019). Synaptic encoding of fear memories in the amygdala. Curr. Opin. Neurobiol 54, 54–59. [PubMed: 30216780]

Sadler KE, McQuaid NA, Cox AC, Behun MN, Trouten AM, and Kolber BJ (2017). Divergent functions of the left and right central amygdala in visceral nociception. Pain 158, 747–759. [PubMed: 28225716]

Sanford CA, Soden ME, Baird MA, Miller SM, Schulkin J, Palmiter RD, Clark M, and Zweifel LS (2017). A central amygdala CRF circuit facilitates learning about weak threats. Neuron 93, 164–178. [PubMed: 28017470]

Sarhan M, Freund-Mercier MJ, and Veinante P (2005). Branching patterns of parabrachial neurons projecting to the central extended amgydala: single axonal reconstructions. J. Comp. Neurol 491, 418–442. [PubMed: 16175547]

Schiess MC, Callahan PM, and Zheng H (1999). Characterization of the electrophysiological and morphological properties of rat central amygdala neurons in vitro. J. Neurosci. Res 58, 663–673. [PubMed: 10561694]

Sugimura YK, Takahashi Y, Watabe AM, and Kato F (2016). Synaptic and network consequences of monosynaptic nociceptive inputs of parabrachial nucleus origin in the central amygdala. J. Neurophysiol 115, 2721–2739. [PubMed: 26888105]

Thompson JM, and Neugebauer V (2017). Amygdala plasticity and pain. Pain Res. Manag 2017, 8296501. [PubMed: 29302197]

Veinante P, Yalcin I, and Barrot M (2013). The amygdala between sensation and affect: a role in pain. J. Mol. Psychiatry 1, 9. [PubMed: 25408902]

Xie JY, De Felice M, Kopruszinski CM, Eyde N, LaVigne J, Remeniuk B, Hernandez P, Yue X, Goshima N, Ossipov M, et al. (2017). Kappa opioid receptor antagonists: a possible new class of therapeutics for migraine prevention. Cephalalgia 37, 780–794. [PubMed: 28376659]

Yalcin I, Bohren Y, Waltisperger E, Sage-Ciocca D, Yin JC, Freund-Mercier MJ, and Barrot M (2011).A time-dependent history of mood disorders in a murine model of neuropathic pain. Biol. Psychiatry 70, 946–953. [PubMed: 21890110]

Yu K, Garcia da Silva P, Albeanu DF, and Li B (2016). Central amygdala somatostatin neurons gate passive and active defensive behaviors. J. Neurosci 36, 6488–6496. [PubMed: 27307236]

Yu K, Ahrens S, Zhang X, Schiff H, Ramakrishnan C, Fenno L, Deisseroth K, Zhao F, Luo MH, Gong L, et al. (2017). The central amygdala controls learning in the lateral amygdala. Nat. Neurosci 20, 1680–1685. [PubMed: 29184202]

Zald DH (2003). The human amygdala and the emotional evaluation of sensory stimuli. Brain Res. Brain Res. Rev 41, 88–123. [PubMed: 12505650]

Zhao S, Ting JT, Atallah HE, Qiu L, Tan J, Gloss B, Augustine GJ, Deisseroth K, Luo M, Graybiel AM, and Feng G (2011). Cell type–specific channelrhodopsin-2 transgenic mice for optogenetic dissection of neural circuitry function. Nat. Methods 8, 745–752. [PubMed: 21985008]

Highlights

- The CeA can both attenuate and exacerbate pain-related behaviors in mice
- Injury induces cell-type-specific bidirectional changes in excitability in the CeA
- Increased firing in CeA-PKCδ neurons drives amplification of pain-related responses
- Activation of CeA-Som neurons attenuates injury-induced pain-related behaviors

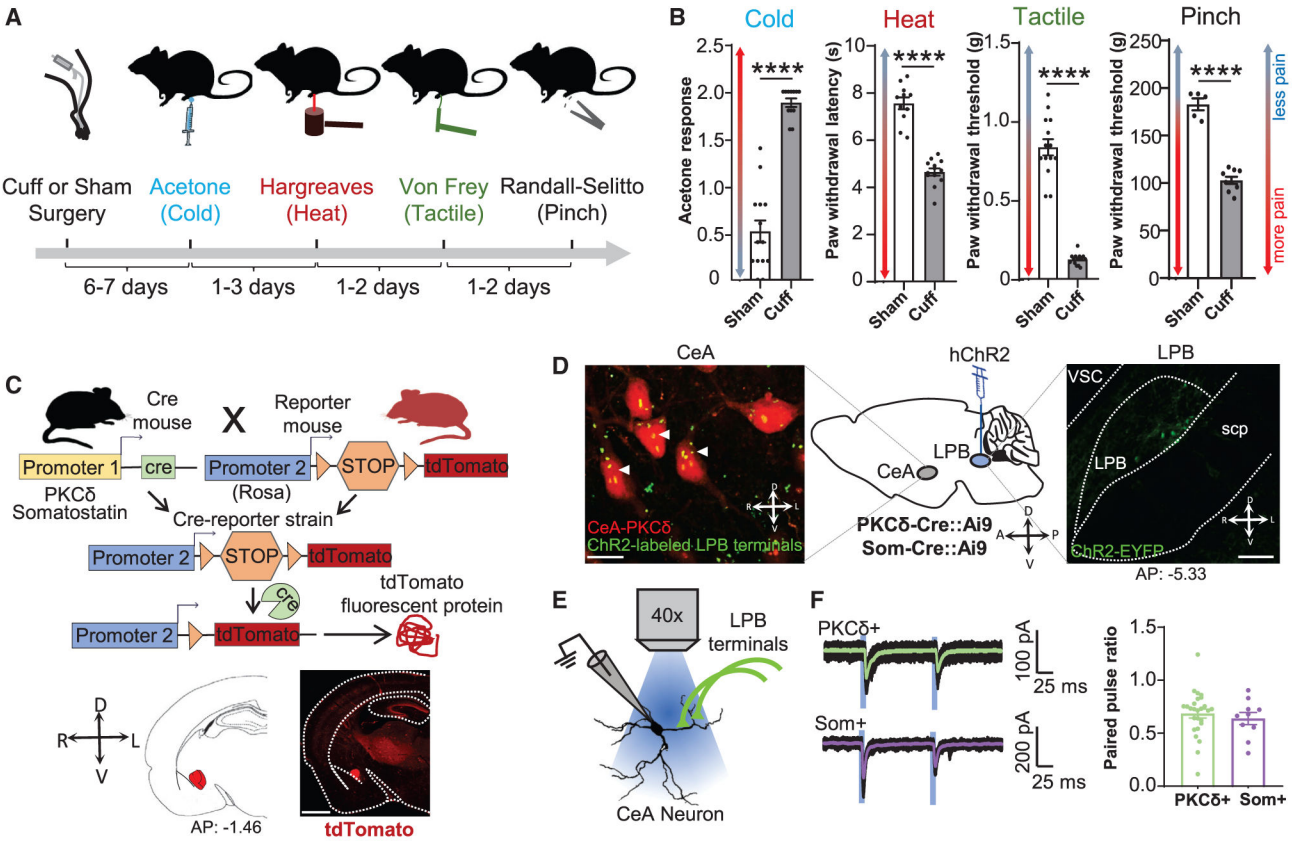

Figure 1. Rodent Model of Neuropathic Pain and Genetic Strategy to Study CeA Cell Types

(A) Timeline of behavioral assays. The sciatic nerve cuff model of neuropathic pain was used with the acetone test, Hargreaves test, von Frey filaments assay, and Randall-Selitto test to assess sensitivity to cold, heat, tactile, and pinch stimulation, respectively.

(B) Mean ± SEM response, withdrawal latency, or withdrawal threshold in response to acetone, heat, tactile, or pinch stimulation of the hindpaw ipsilateral to sciatic nerve treatment in sham and cuff mice (n = 14 sham and 12 cuff for acetone test; n = 11 sham and 13 cuff for Hargreaves test; n = 14 sham and 14 cuff for von Frey filaments test; n = 9 sham and 5 cuff for Randall-Selitto; ****$p < 0.0001$; unpaired t test).

(C) A schematic of the experimental approach to fluorescently label CeA-PKCδ and CeA-Som cells. *Prkcd*-Cre or *Sst*-Cre mice were crossed with Ai9 reporter mice. The offspring expresses tdTomato in CeA-PKCδ or CeA-Som cells. Left bottom panel shows a diagram of a coronal brain section containing the CeA, highlighted in red (modified from Paxinos and Franklin, 2001). Right bottom panel depicts a representative image of a coronal mouse brain section from a *Prkcd*-Cre::Ai9 mouse depicting tdTomato-positive cells in red. Scale bar, 1,000 μm.

(D) Center panel shows a schematic of the experimental approach. *Prkcd*-Cre::Ai9 or *Sst*-Cre::Ai9 mice were stereotaxically injected with AAV2-hsyn-hChR2(H134R)-EYFP into the lateral parabrachial nucleus (LPB). Right panel depicts a representative image of a coronal mouse brain slice containing the LPB of a *Prkcd*-Cre::Ai9 mouse injected with AAV2-hsyn-hChR2(H134R)-EYFP into the LPB. Localization of transduced cells within the LPB is shown in green. Left image depicts representative image of a coronal mouse brain slice

containing the CeA of a *Prkcd*-Cre::Ai9 mouse injected with AAV2-hsyn-hChR2(H134R)-EYFP into the LPB. tdTomato-positive cells are shown in red, and axonal terminals from the PB are shown in green. Arrowheads depict LPB terminals colocalizing with CeA-PKCδ cells. Scale bars are 10 μm (left panel) and 100 μm (right panel).

(E) Schematic of the whole-cell voltage-clamp recordings performed on CeA cells receiving LPB inputs. 470-nm light stimulates the LPB terminals.

(F) Representative traces of whole-cell voltage-clamp recordings obtained from tdTomato-positive CeA neurons in response to blue light stimulation (duration, 5 ms). Ten overlaid PKCδ- or Som-positive responses are shown in black and the averaged response in green or purple, respectively. The blue bars represent the timing and duration of blue light stimulation. Mean ± SEM of paired pulse ratios between the first and second light pulse (n = 26 CeA-PKCδ and 10 CeA-Som neurons).

See also Figure S1 and Table S1.

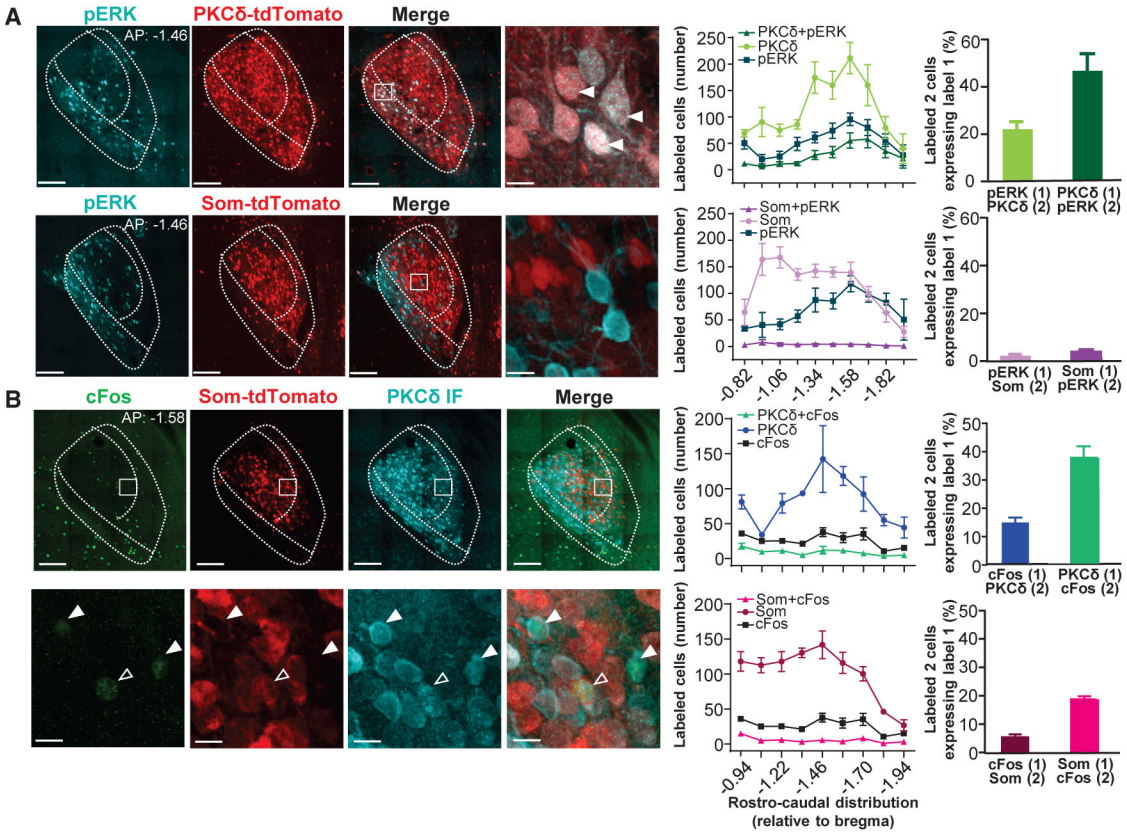

Figure 2. Nerve-Injury-Induced ERK Activation and c-Fos Expression Is Preferentially Localized to CeA-PKCδ Neurons

(A) Representative images of coronal brain slices containing the CeA and immunostained for pERK (cyan) 1 week following cuff implantation on the sciatic nerve. Cells positive for PKCδ-tdTomato (top) or *Sst*-tdTomato (bottom) are shown in red. Low- and high-magnification images of the merged signals between pERK and PKCδ-tdTomato (arrowheads) or *Sst*-tdTomato are shown on the right panels. Colocalization of pERK and PKCδ expression are denoted with solid arrows. Rostro-caudal distribution of labeled cells and mean ± SEM percentage of cells co-labeled for pERK and PKCδ-tdTomato (top panel) or pERK and *Sst*-tdTomato (bottom panel) are shown on the right (n = 5 mice, four to seven slices per mouse).

(B) c-Fos expression in the CeA in response to pinching of the hindpaw ipsilateral to sciatic nerve cuff. Representative low- (top) and high-magnification (bottom) images of coronal brain slices containing the CeA and immunostained for c-Fos (green) and PKCδ (cyan). Cells positive for *Sst*-tdTomato are shown in red. Merged signals are shown on the right panels. Colocalization of c-Fos and PKCδ expression are denoted with solid arrows and colocalization between c-Fos and *Sst*-tdTomato with open arrows. Rostro-caudal distribution of labeled cells and mean ± SEM percentage of cells co-labeled with c-Fos and PKCδ (top panel) or c-Fos and *Sst*-tdTomato (bottom panel) are shown on the right (n = 4 mice, seven or eight slices per mouse). The white boxes depict the areas in the magnified images. Scale bars represent 100 μM (left panels in A and top panel in B) and 10 μM (right panel in A and

bottom panel in B). Low-magnification images are a montage of 16 images collected using a 40× objective.

See also Figures S1 and S2.

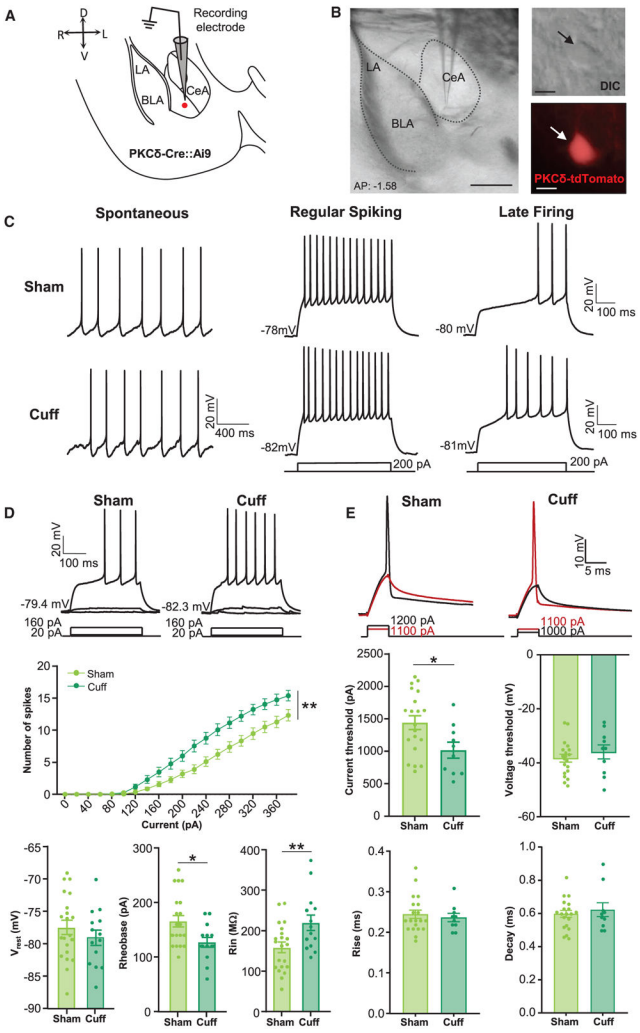

Figure 3. Sciatic Nerve Injury Increases Firing Rates in CeA-PKCδ Neurons

(A) Schematic diagram depicting the anatomical localization of the recording electrode within the CeA in an acute brain slice.

(B) Left panel depicts a representative low-magnification image of an acute brain slice with the recording pipette positioned in the CeA. Right panel shows high-magnification differential interference contrast-enhanced infrared images or fluorescent images of a tdTomato-positive CeA-PKCδ cell (shown in red). Scale bars represent 200 μm (left panel) and 10 μm (right panels).

(C) Representative voltage records of spontaneously active (left), regular-spiking (RS; middle), and late-firing (LF; right) CeA-PKCδ neurons in sham (top) and cuff (bottom) mice. Repetitive firing in regular-spiking and late-firing neurons was evoked in response to a prolonged (500 ms) 200-pA depolarizing current injection; injected current amplitudes are illustrated under the voltage records.

(D) Representative voltage recordings of late-firing CeA-PKCδ neurons in acute slices prepared from sham (left) or cuff (right) mice; repetitive firing was evoked in response to prolonged (500 ms) depolarizing current injections of varying amplitudes; injected current amplitudes are illustrated under the voltage records. Mean ± SEM numbers of action

potentials (middle panel) evoked during 500-ms current injections are plotted as a function of the amplitudes of the injected currents (n = 21 neurons for sham and 14 neurons for cuff; effect of current injection, $F_{(19, 608)} = 283.9$, $p < 0.0001$; effect of treatment, $F_{(1, 32)} = 8.9$, $p = 0.0054$; interaction, $F_{(19, 608)} = 7.3$, $p < 0.0001$; **p = 0.0054 for effect of treatment; two-way ANOVA). Rheobase, input resistances (R_{in}) and resting membrane potentials were analyzed in individual cuff (n = 14) and sham (n = 21) CeA-PKCδ neurons; values are presented as mean ± SEM. **p = 0.0095; *p < 0.05; unpaired t test.

(E) Representative traces of single action potentials generated in response to a 5-ms depolarizing current injection in sham (left) and cuff (right) mice; current and voltage threshold for action potential generation as well as rise and decay times of the action potential were analyzed in individual cuff (n = 10) and sham (n = 20) CeA-PKCδ neurons. Values are presented as mean ± SEM; *p < 0.05; unpaired t test.

See also Figure S3 and Table S1.

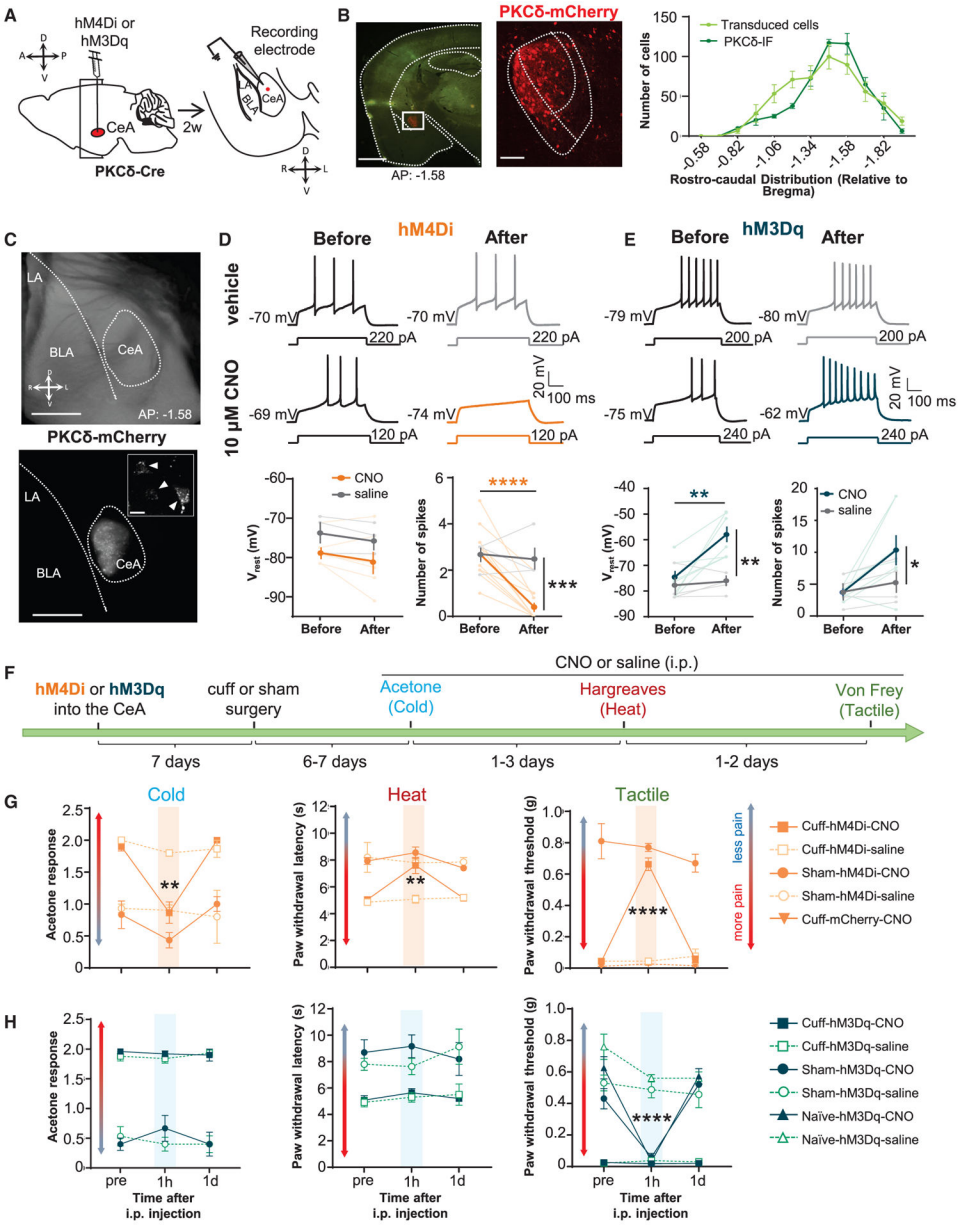

Figure 4. Chemogenetic Inhibition of CeA-PKCδ Cells Reverses Nerve-Injury-Induced Tactile and Thermal Hypersensitivity, while Chemogenetic Excitation Induces Tactile Hypersensitivity

(A) A schematic of the experimental approach. *Prkcd*-Cre mice were stereotaxically injected with AAV-DIO-hM4Di-mCherry, AAV-DIO-hM3Dq-mCherry, or AAV-DIO-mCherry into the amygdala. Current-clamp recordings were obtained from mCherry-CeA-positive cells in acute amygdala slices 2 weeks after the injection.

(B) Representative low- (left) and high-magnification (right) images of a coronal mouse brain slice from a *Prkcd*-Cre mouse injected with AAV-DIO-hM4Di-mCherry into the CeA. The green fluorescent channel is overexposed to facilitate visualization of the anatomical landmarks. The white box depicts the area in the magnified image on the right panel. Mean ± SEM number of mCherry-transduced and PKCδ IF-positive cells is shown in the right

panel (n = 19 mice for the transduced cells and 6 mice for the PKCδ-IF cells). Scale bars represent 1,000 μm (left panel) and 100 μm (right panel).

(C) Representative bright-field (top) and fluorescent (bottom) images of an acute amygdala slice obtained from a *Prkcd*-Cre mouse stereotaxically injected with AAV-DIO-hM4Di-mCherry are shown at the bottom. Inset shows a magnified view of transduced cells, denoted with the solid arrowheads. Scale bars represent 200 μm (main panels) and 10 μm (inset).

(D) Representative traces of whole-cell current-clamp recordings obtained from CeA neurons transduced with hM4Di-mCherry before (left) and after (right) bath application of 10 μM CNO (bottom) or vehicle (top). Action potentials were elicited using a 500-ms depolarizing current injection that evoked three to six action potentials before the bath application. The same magnitude of depolarizing current injection was used before and after bath application. Mean ± SEM resting membrane potential and number of evoked spikes before and after bath application are shown (n = 4 saline and 14 CNO cells; effect of time, $F_{(1, 16)} = 21.0$, p = 0.0003; effect of treatment, $F_{(1, 16)} = 7.0$, p = 0.0180; interaction, $F_{(1, 16)} = 14.9$, p = 0.0014; ***p = 0.0003 for saline versus CNO after bath application; two-way ANOVA followed by Sidak's multiple comparisons test).

(E) Representative traces of whole-cell current-clamp recordings obtained from CeA neurons transduced with hM3Dq-mCherry before (left) and after (right) bath application of 10 μM CNO (bottom) or vehicle (top). Mean ± SEM resting membrane potential (V_{rest}) and number of evoked spikes before and after bath application. n = 4 saline and 7 CNO cells; for V_{rest}: effect of time, $F_{(1, 9)} = 9.3$, p = 0.0139; effect of treatment, $F_{(1, 9)} = 10.0$, p = 0.0119; interaction, $F_{(1, 9)} = 6.4$, p = 0.0325; **p = 0.0016 for saline versus CNO after bath application; two-way ANOVA followed by Sidak's multiple comparisons test; for number of action potentials: effect of time, $F_{(1, 9)} = 5.7$, p = 0.0408; effect of treatment, $F_{(1, 9)} = 1.6$, p = 0.2423; interaction, $F_{(1, 9)} = 2.4$, p = 0.1590; *p = 0.0198 for before versus after CNO bath application; two-way ANOVA followed by Sidak's multiple comparisons test.

(F) Experimental timeline for behavioral experiments.

(G) Mean ± SEM acetone response, withdrawal latency, and withdrawal thresholds in the hindpaw ipsilateral to sciatic nerve treatment before and 1 h and 1 day after CNO (or vehicle) i.p. injection in cuff or sham mice stereotaxically injected with either AAV-DIO-hM4Di-mCherry or AAV-DIO-mCherry into the CeA (acetone test: n = 6 per treatment, **p = 0.0068 for pre-injection versus 1 h after CNO in cuff-hM4Di-CNO; Hargreaves test: n = 3 sham-saline, 5 cuff-saline; 6 sham-CNO and 4 cuff-CNO, **p = 0.0022 for pre-injection versus 1 h after CNO in cuff-hM4Di-CNO; von Frey test: n = 7 cuff-hM4Di-CNO, 5 cuff-hM4Di-Sal, 4 sham-hM4Di-CNO, 2 sham-hM4Di-Sal, 4 cuff-mCherry-CNO, ****p < 0.0001 for pre-injection versus 1 h after CNO in cuff-hM4Di-CNO, two-way ANOVA followed by Dunnett's multiple comparisons test).

(H) Mean ± SEM acetone response, withdrawal latency, and withdrawal thresholds in the hindpaw ipsilateral to sciatic nerve treatment before and 1 h and 1 day after CNO (or vehicle) i.p. injection in cuff, sham, or naive mice stereotaxically injected with AAV-DIO-hM3Dq-mCherry into the CeA (acetone test: n = 6 sham and 5 cuff; Hargreaves test: n = 7 sham-saline, 7 cuff-saline; 5 sham-CNO and 7 cuff-CNO; von Frey test: n = 3 naive, 6 cuff, 4 sham, ****p < 0.0001 for pre-injection versus 1 h after CNO in naive-hM3Dq-CNO and sham-hM3Dq-CNO, two-way ANOVA followed by Dunnett's multiple comparisons test). See also Figures S4 and S5.

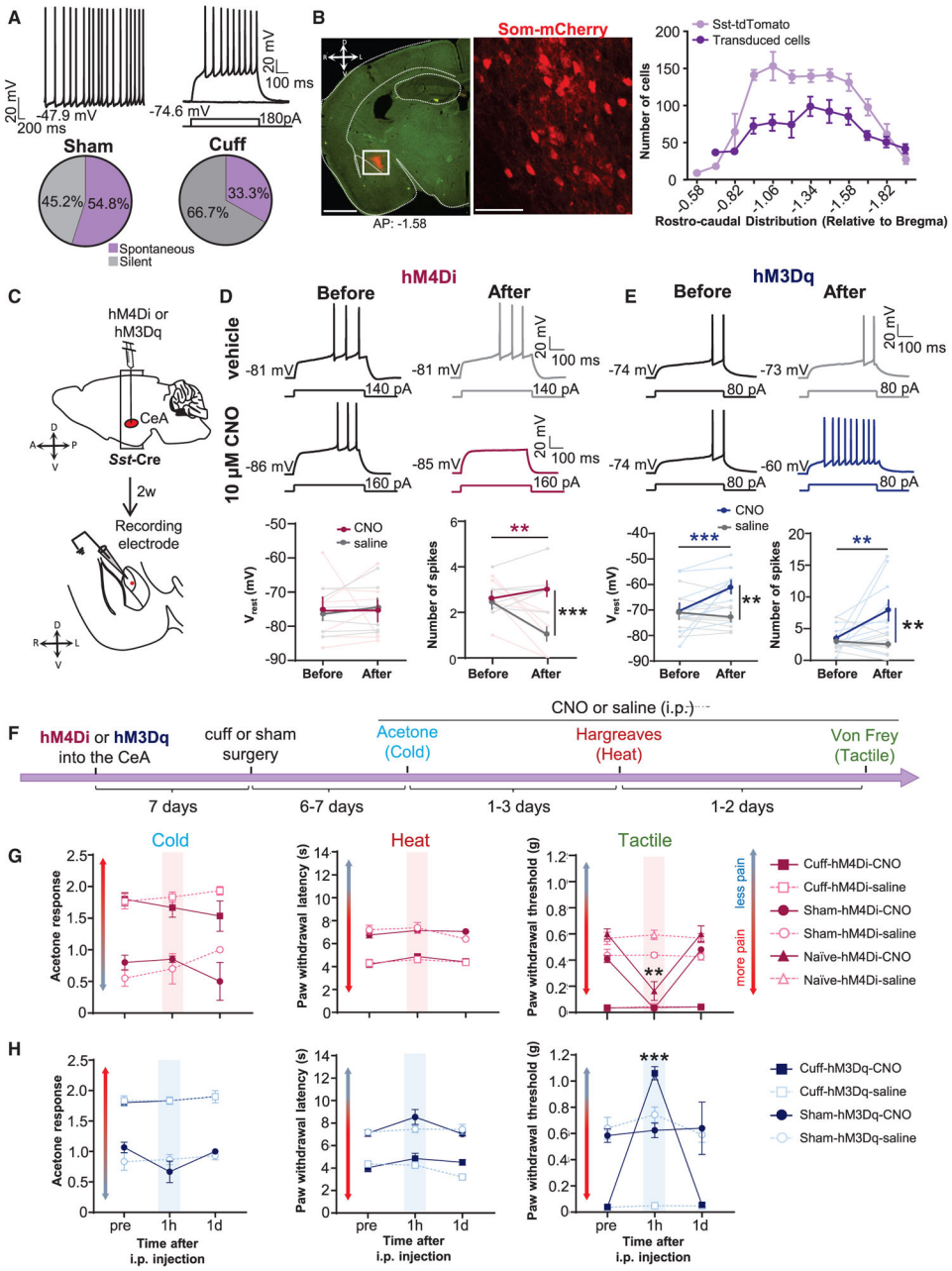

Figure 5. Silencing of CeA-Som Neurons Elicits Peripheral Tactile Hypersensitivity in Naive, Uninjured Mice, while Chemogenetic Excitation Reverses Tactile Hypersensitivity in Injured Mice

(A) Representative voltage records of CeA-Som neurons that were spontaneously active (left panel) or silent at rest and fired repetitively in response to depolarizing current injection (right panel); injected current amplitudes are illustrated under the voltage records. The proportion of spontaneous CeA-Som neurons was significantly higher in sham conditions than in cuff conditions (n = 31 sham neurons and 42 cuff neurons; p = 0.0331; chi-square test).

(B) Representative low- (left) and high-magnification (right) images of a coronal mouse brain slice from a *Sst*-Cre mouse injected with AAV-DIO-hM4Di-mCherry into the CeA. The green fluorescent channel is overexposed to facilitate visualization of the anatomical landmarks. The white box depicts the area in the magnified image on the right panel. Mean ± SEM number of mCherry-transduced and *Sst*-tdTomato labeled cells is shown in the right panel (n = 9 mice for the transduced cells and 5 mice for the *Sst*-tdTomato cells). Scale bars represent 1,000 μm (left panel) and 50 μm (right panel).

(C) A schematic of the experimental approach for the electrophysiological experiments. *Sst*-Cre mice were stereotaxically injected with AAV-DIO-hM4Di-mCherry or AAV-DIO-hM3Dq-mCherry into the amygdala. Current-clamp recordings were obtained from mCherry-CeA-positive cells in acute amygdala slices 2 weeks after the injection.

(D) Representative traces of whole-cell current-clamp recordings obtained from CeA neurons transduced with hM4Di-mCherry before (left) and after (right) bath application of 10 μM CNO (bottom) or vehicle (top). Action potentials were elicited using a 500-ms depolarizing current injection that elicited three to six action potentials. The same magnitude of depolarizing current injection was used before and after bath application. Mean ± SEM resting membrane potential and number of evoked spikes before and after bath application are shown (n = 6 saline and 7 CNO cells; effect of time, $F_{(1, 11)} = 5.0$, $p = 0.0472$; effect of treatment, $F_{(1, 11)} = 6.4$, $p = 0.0281$; interaction, $F_{(1, 11)} = 16.2$, $p = 0.0020$; ***$p = 0.0009$ for saline versus CNO after bath application; two-way ANOVA followed by Sidak's multiple comparisons test).

(E) Representative traces of whole-cell current-clamp recordings obtained from CeA neurons transduced with hM3Dq-mCherry before (left) and after (right) bath application of 10 μM CNO (bottom) or vehicle (top). Mean ± SEM resting membrane potential and number of evoked spikes before and after bath application are shown (n = 8 saline and 10 CNO cells; effect of time, $F_{(1, 16)} = 6.7$, $p = 0.0199$; effect of treatment, $F_{(1, 16)} = 3.1$, $p = 0.0968$; interaction, $F_{(1, 16)} = 12.3$, $p = 0.0029$; **$p = 0.0091$ for saline versus CNO after bath application; two-way ANOVA followed by Sidak's multiple comparisons test.

(F) Experimental timeline for behavioral experiments.

(G) Mean ± SEM acetone response, withdrawal latency, and withdrawal thresholds in the hindpaw ipsilateral to sciatic nerve treatment before and 1 h and 1 day after CNO (or vehicle) i.p. injection in cuff, sham, or naive mice stereotaxically injected with AAV-DIO-hM4Di-mCherry into the CeA (acetone and Hargreaves tests: n = 6 cuff and 4 sham; von Frey test: n = 6 naive-hM4Di-saline, 7 naive-hM4Di-CNO, 6 cuff per treatment and 4 sham per treatment, **$p < 0.01$ for pre-injection versus 1 h after CNO in sham and naive mice, two-way ANOVA followed by Dunnett's multiple comparisons test).

(H) Mean ± SEM acetone response, withdrawal latency, and withdrawal thresholds in the hindpaw ipsilateral to sciatic nerve treatment before and 1 h and 1 day after CNO (or vehicle) i.p. injection in cuff, sham, or naive mice stereotaxically injected with AAV-DIO-hM3Dq-mCherry into the CeA (acetone test: n = 6 sham and 6 cuff; Hargreaves test: n = 8 sham-saline, 7 sham-CNO, and 6 cuff per treatment; von Frey test: n = 4 cuff and 5 sham per treatment, ***$p = 0.0004$ for pre-injection versus 1 h after CNO in cuff-hM3Dq-CNO, two-way ANOVA followed by Dunnett's multiple comparisons test).

See also Figures S3, S4, and S6 and Table S1.

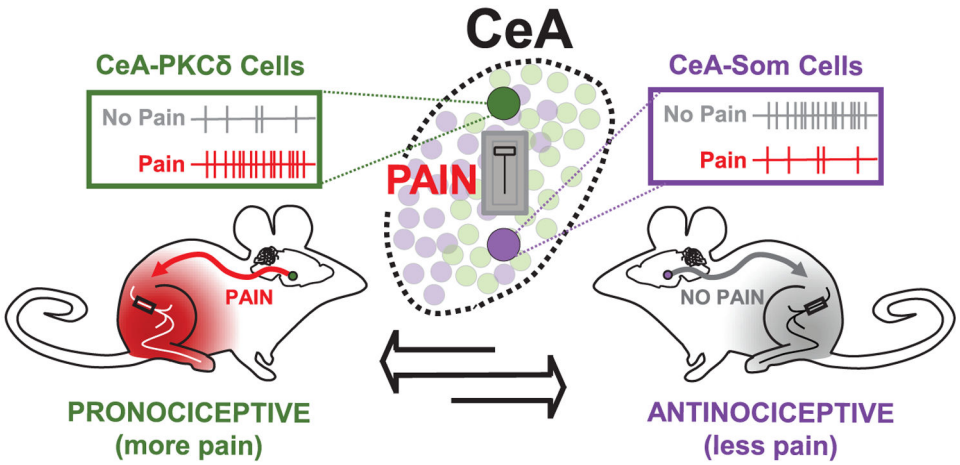

Figure 6. Proposed Model for Dual and Opposing Modulation of Pain-Related Behaviors in the CeA

The CeA functions as a pain rheostat, attenuating or exacerbating pain-related behaviors in mice. The dual and opposing function of the CeA is encoded by opposing injury-induced changes in the excitability CeA-PKCδ (green, left) and CeA-Som (purple, right) cells, with increases in firing in CeA-PKCδ neurons and attenuation of excitability in CeA-Som cells following injury. Activation of these two populations of CeA cells promotes completely opposite behaviors, with activation of CeA-PKCδ cells driving increases in pain (pronociception) and activation of CeA-Som neurons resulting in decreases in pain (antinociception).

KEY RESOURCES TABLE

REAGENT or RESOURCE	SOURCE	IDENTIFIER
Antibodies		
rat anti-mCherry	Invitrogen	Cat# M11217; RRID:AB_2536611
rabbit anti-Phospho-p44/42 MAPK (Erk1/2)	Cell Signaling Technology	Cat# 9101; RRID:AB_331646
rabbit anti-Phospho-c-Fos (Ser32)	Cell Signaling Technology	Cat# 5348; RRID:AB_10557109
Rabbit anti-GFP	Invitrogen	Cat# A-6455; RRID:AB_221570
mouse anti-PKCδ	BD Biosciences	Cat# 610397; RRID:AB_397780
goat anti-rat Cy3	Invitrogen	Cat# A10522; RRID:AB_2534031
Alexa Fluor 647-conjugated goat anti-rabbit	Invitrogen	Cat# A-21244; RRID:AB_2535812
Alexa Fluor 647-conjugated goat anti-mouse	Invitrogen	Cat# A-21235; RRID:AB_2535804
Goat anti-Rabbit IgG (H+L) Highly Cross-Adsorbed Secondary Antibody, Alexa Fluor 488	Invitrogen	Cat# A-11034; RRID:AB_2576217
Bacterial and Virus Strains		
AAV8-hSyn-DIO-hM4Di-mCherry	Krashes et al., 2011	Addgene viral prep # 44362-AAV8
AAV8-hSyn-DIO-mCherry	Roth lab DREADDs (unpublished)	Addgene viral prep # 50459-AAV8
pAAV-hSyn-DIO-hM3D(Gq)-mCherry	Krashes et al., 2011	Addgene viral prep #44361-AAV8
AAV2-hsyn-hChR2(H134R)-EYFP	UNC Vector core	Lot Number AV4384G
Experimental Models: Organisms/Strains		
Prkcd-cre mice	GENSAT	founder line 011559-UCD
Swiss-Webster mice	Taconic Farms	SW- SW-M
Ai9 mice	Jackson Laboratories	Ai9- 007909
heterozygous male *Sst*-cre	Jackson Laboratory	founder line 018973
female C57BL/6NJ	Jackson Laboratory	C57BL/6NJ- 005304
Oligonucleotides		
Forward primer to genotype for the presence of cre-recombinase: TTAATCCATATTGGCAGAACGAAAACG	Transnetyx	https://www.transnetyx.com/
Reverse primer to genotype for the presence of cre-recombinase: CAGGCTAAGTGCCTTCTCTACA	Transnetyx	https://www.transnetyx.com/